Assessing Porphyry Copper Deposit Fertility in British Columbia Batholiths using Zircons

Farhad Bouzari, Craig J.R. Hart, and Thomas Bissig

Geoscience BC Report 2020-08

MDRU Publication 450

Geoscience BC

MDRU
MINERAL DEPOSIT RESEARCH UNIT

UBC THE UNIVERSITY OF BRITISH COLUMBIA

Assessing Porphyry Copper Deposit Fertility in British Columbia Batholiths using Zircons

Farhad Bouzari[1], Craig J.R. Hart[1], and Thomas Bissig[2]

Geoscience BC* Report 2020-08

MDRU Publication 450

[1] MDRU–Mineral Deposit Research Unit, Department of Earth, Ocean and Atmospheric Sciences, The University of British Columbia, Vancouver, BC

[2] Bissig Geoscience Consulting, Vancouver, BC

Keywords: porphyry deposit, fertility, zircon, British Columbia

Suggested Citation:
Bouzari, F., Hart, C.J.R. and Bissig, T. (2020). Assessing British Columbia Porphyry Fertility in British Columbia Batholiths using Zircons. Geoscience BC Report 2020-08, MDRU Publication 450, 24p.

Report prepared by MDRU†

Department of Earth, Ocean and Atmospheric Sciences
The University of British Columbia
Vancouver, BC V6T 1Z4, Canada
Tel: +1-604-822-6136
Email: mdru@eoas.ubc.ca

Includes bibliographic references.
Electronic monograph issued in PDF format.
ISBN 978-0-88865-453-3

*Geoscience BC is an independent, non-profit organization that generates earth science in collaboration with First Nations, local communities, government, academia and the resource sector. Our independent earth science enables informed resource management decisions and attracts investment and jobs. Geoscience BC gratefully acknowledges the financial support of the Province of British Columbia.

†MDRU–Mineral Deposit Research Unit is an internationally-recognized collaborative venture between the mining industry and Earth, Ocean and Atmospheric Sciences Department at The University of British Columbia (UBC), established with assistance from the Natural Sciences and Engineering Research Council of Canada (NSERC), and devoted to solving mineral exploration-related problems.

Cover image: Cathodoluminescence image of zircon grains showing fertility secrets of BC's porphyry plutons. British Columbia geology map courtesy of Cui, Y., Miller, D., Schiarizza, P., and Diakow, L.J., 2017. British Columbia digital geology. British Columbia Ministry of Energy, Mines and Petroleum Resources, British Columbia Geological Survey Open File 2017-8, 9p. Data version 2019-12-19.

ABSTRACT

Porphyry copper deposits in British Columbia occur within or around the edges of large batholiths composed of nonmineralized and fewer mineralized plutons. Identifying porphyry-fertile plutons and distinguishing them from barren plutons provides a significant advantage to exploration geologists seeking to discover porphyry copper deposits. Trace-element composition of zircon, a common accessory mineral in granitoid rocks, provides clues to the magmatic-hydrothermal history of magmas capable of generating porphyry copper deposits. This study identifies and characterizes the chemical signatures of copper ore-forming processes in zircon from selected plutonic lithologies that form the Guichon Creek, Takomkane, Granite Mountain and Toodoggone batholiths, and develops tools and strategies for the exploration of porphyry copper deposits in magmatic belts. A total of 1021 zircon grains from 42 rock samples representing various phases of each batholith were analyzed. Cathodoluminescence (CL) microscopy was used to document texture and zoning characteristics of zircon grains and 1397 spots were analyzed by EPMA and LA-ICP-MS for trace-element characterization.

Results show that porphyry-fertile Late Triassic and Early Jurassic plutons in BC have several distinct characteristics that indicate an increased potential to generate porphyry copper deposits. Zircons from mineralized phases have low Th/U and high Yb/Gd ratios that suggest fertile magmas were formed after certain amounts of fractional crystallization. Similarly, Ti-in-zircon temperatures show that these plutons yield lower model temperatures of ca. 750°C to 600°C consistent with zircon crystallization in near-eutectic conditions close to the solidus of hydrous granite.

Zircons from the mineralized plutons have small negative Eu anomalies (Eu_N/Eu_N^* ≥0.35) whereas nonmineralized plutons show variable Eu anomalies, which is interpreted to be largely controlled by crystal fractionation, particularly that of apatite and titanite. The crystal fractionation of magmas alone does not produce ore deposits if the magma has a low oxidation state or low magmatic water content, or both. The porphyry-fertile plutons have zircons with Eu anomaly values that are not significantly affected by Hf concentration or Yb/Gd values, proxies for crystal fractionation, suggesting that the oxidation state and magmatic water remained significantly high during the cooling history of the magma. This key fertility feature has been interpreted to reflect SO_2 degassing and subsequent increased oxidation of parental porphyry melts (Dilles et al., 2015).

Our study, for the first time, shows that zircon texture correlates with its chemical fertility indices. Zircons from fertile plutons characterized by oxidized (Eu anomaly >0.35), cooled (<750°C) evolved (Hf >9000 ppm) wet magmas, commonly show oscillatory zoning with minimal irregular texture at rims, whereas, nonmineralized plutons commonly contain zircon with tabular or oscillatory zoning and irregular texture characterized by new growth zones crosscutting older zones. The tabular zircons are more common in older plutons (>195 Ma) and we interpret that zircons with irregular oscillatory zoning are common in hotter (above eutectic) melts. These chemical and textural features of zircon along with other porphyry indicator minerals such as apatite and titanite (Bouzari et al., 2018) provide new tools to evaluate porphyry potential of BC's plutonic rocks.

1. INTRODUCTION

Porphyry copper deposits are critical contributors to the British Columbia (BC) economy. BC is Canada's largest producer of copper with more than $2 billion generated annually from copper concentrate revenues won from BC porphyry copper deposits (PwC Canada, PricewaterhouseCoopers, 2019). The economic benefits of a new porphyry copper deposit discovery cannot be overstated.

Information that improves an exploration geologist's ability to quickly determine porphyry copper prospective regions of BC, or more specifically what igneous rocks are more likely to generate a porphyry copper deposit, is more likely to result in exploration success with a discovery. Thus, tools that aid in distinguishing metal-fertile from barren plutons provide a significant advantage to exploration geologists' decision-making. This is particularly the case in BC, where many porphyry copper deposits formed within or around the edges of large composite granitoid batholiths, and the potential of individual rock bodies could be evaluated.

Zircon ($Zr[Hf]SiO_4$) is a common accessory mineral in granitoid rocks including those that generate and host porphyry copper deposits. Although the isotopic compositions of zircons have long been utilized to provide a chronometer that indicates the age of the rock, recent research increasingly indicates that the range of physical and chemical characteristics of zircons records the evolution of its host magma and can provide information on that magma's ability to generate a porphyry copper deposit. This porphyry copper mineralizing potential is known as fertility and it may be possible to identify those highly fertile intrusions in BC based on their zircon characteristics.

The physical characteristics of zircons such as size, shape, inclusions and internal zoning can be reasonably determined with various microscopic methods including optical microscopy, scanning electron microscopy and cathodoluminescence imaging. However, measuring the chemical features of the mineral grains requires microanalytical techniques such as electron microprobes, or ion probes and lasers that are connected to mass spectrometers. In particular, the development of stable, rapid, high-resolution laser-ablation inductively coupled plasma-mass spectrometry (LA-ICP-MS) analysis on zircon has led to an enormous increase in the amount of high-quality isotopic and trace-element data that geochemists and petrologists can access to assist them in resolving problems associated with the geology of igneous and metamorphic rocks (Jackson et al., 2003).

This study investigates district- to batholith-scale porphyry copper deposit fertility indicators in zircons in four regions of British Columbia: the Guichon Creek, Takomkane and Granite Mountain batholiths, as well as the Toodoggone area (Fig. 1). In each area, textural and geochemical features of zircons are characterized, and these results are used to develop tools and strategies to improve exploration success for porphyry copper deposits in these regions of BC. Results show that textural as well as geochemical characteristics contribute to distinguishing porphyry-fertile from nonmineralized or poorly mineralized plutons.

2. PORPHYRY-FERTILE MAGMAS AND ZIRCONS

Porphyry copper deposits form from hydrothermal fluids that exsolve from magma in large crystallizing batholiths (Burnham and Ohmoto, 1980; Dilles and Einaudi, 1992). These fluids accumulate Cl, S and metals that preferentially partition from the magma to the fluid. As these fluids rise and rapidly expand, they fracture the host rocks thus increasing fluid-rock interactions and decreasing the fluid's temperature which results in episodic deposition of the silicate and sulphide minerals that form porphyry copper deposits. Six key parameters (Burnham and Ohmoto, 1980; Audétat and Simon, 2012) influence a magma's ability to form porphyry copper deposits: (1) oxidation state, (2) temperature, (3) water, (4) metal, (5) chlorine and (6) sulphur content.

Zircon is a robust accessory mineral that records physical and geochemical processes and evolution of most crystallizing granitoid magmas, including those that form porphyry copper deposits. Zircon commonly has detailed internal textures and zoning that provide clues to the environment and processes in which it formed (Gagnevin et al., 2010). The crystallization

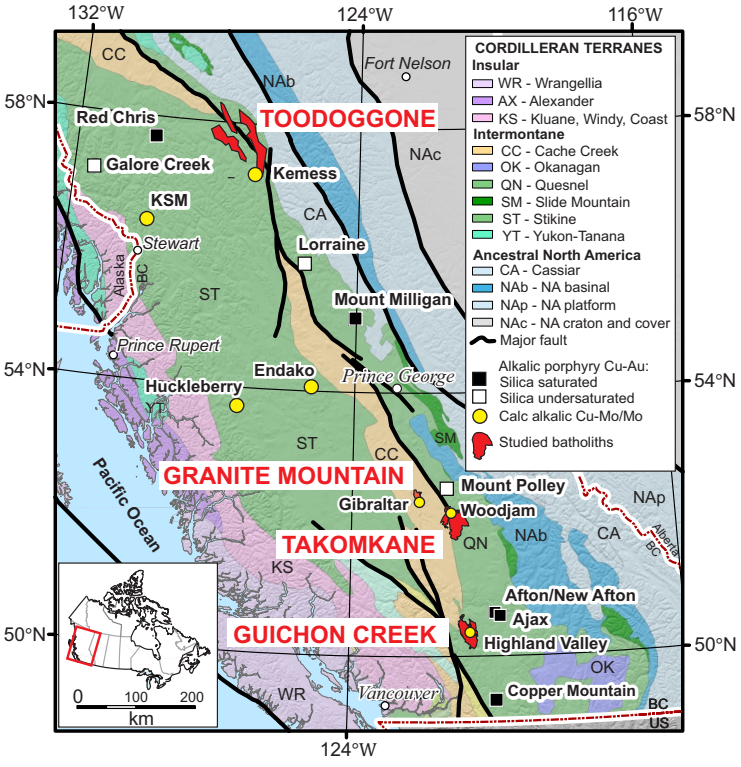

Figure 1: Location map, showing Cordilleran terranes, studied batholiths and major porphyry copper deposits in British Columbia (modified from Bissig and Cooke, 2014).

history of zircons provides unique insights into magma petrogenesis. These insights are particularly well illuminated with cathodoluminescence (CL) imaging which responds to subtle changes in mineral character and characteristics (Hanchar and Miller, 1993). Zircon textures illuminated with CL imaging and coupled with the power of geochemical analyses by LA-ICP-MS are best to determine the complex magmatic histories (Hanchar and Miller, 1993; Wark and Miller, 1993; Gagnevin et al., 2010).

The zircon mineral structure can incorporate trace elements such as Eu, Ce and Ti and their variations can be used to estimate oxidation state and temperature of the parental magma (Lee et al., 2017b). The chemical composition of zircon has been used to elaborate many magmatic processes, including crystal fractionation (Thomas et al., 2002; Lowery Claiborne et al., 2006), interaction with hydrothermal fluids (Thomas et al., 2002; Hoskin, 2005), magma mixing (Wang et al., 2002) and a potential source indicator (Belousova et al., 2002).

The trace element compositions of zircon can also be used to determine the temperature and oxidation state of the parental magma. Investigations by Ballard et al. (2002) and Shen et al. (2015) correlated the relative uptake of Ce^{4+}/Ce^{3+} in zircon with the oxidation state of barren and fertile porphyry copper-mineralized intrusive rocks in northern Chile and Central Asia. Dilles et al. (2015), Lee et al. (2017b) and Banik et al. (2017) showed similar relationships for porphyry copper deposits in Chile and Nevada using the Eu concentration in zircon. Furthermore, Shen et al. (2015), and Shu et al. (2019) demonstrated a correlation between zircon Ce^{4+}/Ce^{3+} ratios and the size of the porphyry copper deposits in Central Asia and China, respectively. These investigations concluded that zircon provides a most useful tool for evaluating the porphyry copper fertility of plutons.

Not only is zircon an excellent recorder of time and magmatic processes, it is also ideal because it is robust. Zircon is resistant to subsolidus and hydrothermal alteration, and demonstrably retains critically important pre-alteration and pre-mineralization geochemical information. It is particularly useful in evaluating porphyry copper deposits. Additionally, because zircon persists in surficial sediments for tens or hundreds of kilometres beyond the hydrothermal or geochemical footprint of magmatic-porphyry centres (Averill, 2011), it can provide clues that enable detection of porphyry-fertile magmas at substantial distances from their source (Lee et al., 2017a). Zircon recovery from soil, rock and drill core samples is both feasible and affordable. Furthermore, U-Pb and Pb-Pb geochronology of zircon using laser ablation has matured to the extent that it constitutes a preferred method to accurately date mineralized and barren magmas (e.g., Spencer et al., 2016; Chiaradia et al., 2013).

3. GEOLOGICAL SETTING

Much of British Columbia is underlain by Mesozoic island arc and associated accretionary margin assemblages. Among these, the Quesnel terrane in south-central BC is characterized by an Upper Triassic to Lower Jurassic island arc volcano-sedimentary package with numerous contemporaneous plutons and batholiths, some with associated clusters of porphyry copper deposits (Logan and Mihalynuk, 2014). In the southern Quesnel terrane, the arc, plutons and batholiths form three arc-parallel belts that become progressively younger to the east (Schiarizza, 2015). The western Late Triassic plutonic belt is characterized by the large calc-alkaline Guichon Creek and Granite Mountain granodioritic batholiths, which host the Highland Valley and Gibraltar porphyry copper districts, respectively (Fig. 1). The central plutonic belt consists of Late Triassic alkaline plutons that are dominated by monzonitic rocks, including the Copper Mountain, Iron Mask and Mount Polley composite intrusions and related porphyry copper deposits. The easternmost belt consists of several Early Jurassic calc-alkaline granodioritic batholiths such as the Pennask and Takomkane batholiths, which host the Brenda and Woodjam/Southeast Zone porphyry copper deposits, respectively.

Within the current tectonic architecture, Stikine terrane is west of Quesnel terrane, separated from it by the Cache Creek oceanic accretionary complexes. Late Triassic to Early Jurassic plutons that intrude northeastern Stikine terrane have variable compositions and the time-space-lithology classifications that characterize southern Quesnel terrane have not been recognized. The Toodoggone mineral district in northeastern Stikine terrane consists of epithermal, skarn and porphyry style mineralization associated with a range of Late Triassic to Early Jurassic plutonic lithologies.

The geology and the zircon fertility characteristics of the plutonic rocks that comprise the Guichon Creek, Granite Mountain and Takomkane batholiths of Quesnel terrane are evaluated, as well as selected plutons in the Toodoggone mineral district.

3.1 Guichon Creek Batholith

The Late Triassic Guichon Creek batholith is a north-trending, approximately 65 x 30 km body that intruded and thermally metamorphosed the Upper Triassic Nicola Group basaltic to andesitic volcanic and volcaniclastic rocks (McMillan et al., 2009) of the Quesnel terrane, southwest of Kamloops (Fig. 2). The batholith is composite and zoned, with earlier diorite and quartz diorite border phases on the margins that surround progressively younger granodiorite phases towards the centre (Casselman et al., 1995; Byrne et al., 2013; D'Angelo et al., 2017). These mostly concentric phases, from the margins inward, are the Border phase, the Highland Valley phases (consisting of Guichon and Chataway subphases), the Bethlehem phases (consisting of Bethlehem and Skeena subphases) and the Bethsaida phase. The Bethlehem and Skeena subphases, and the Bethsaida phase host most of the Highland Valley porphyry copper-molybdenum deposits (Valley, Lornex, Highmont, Bethlehem and JA). Two mineralization events are recognized: an older Bethlehem

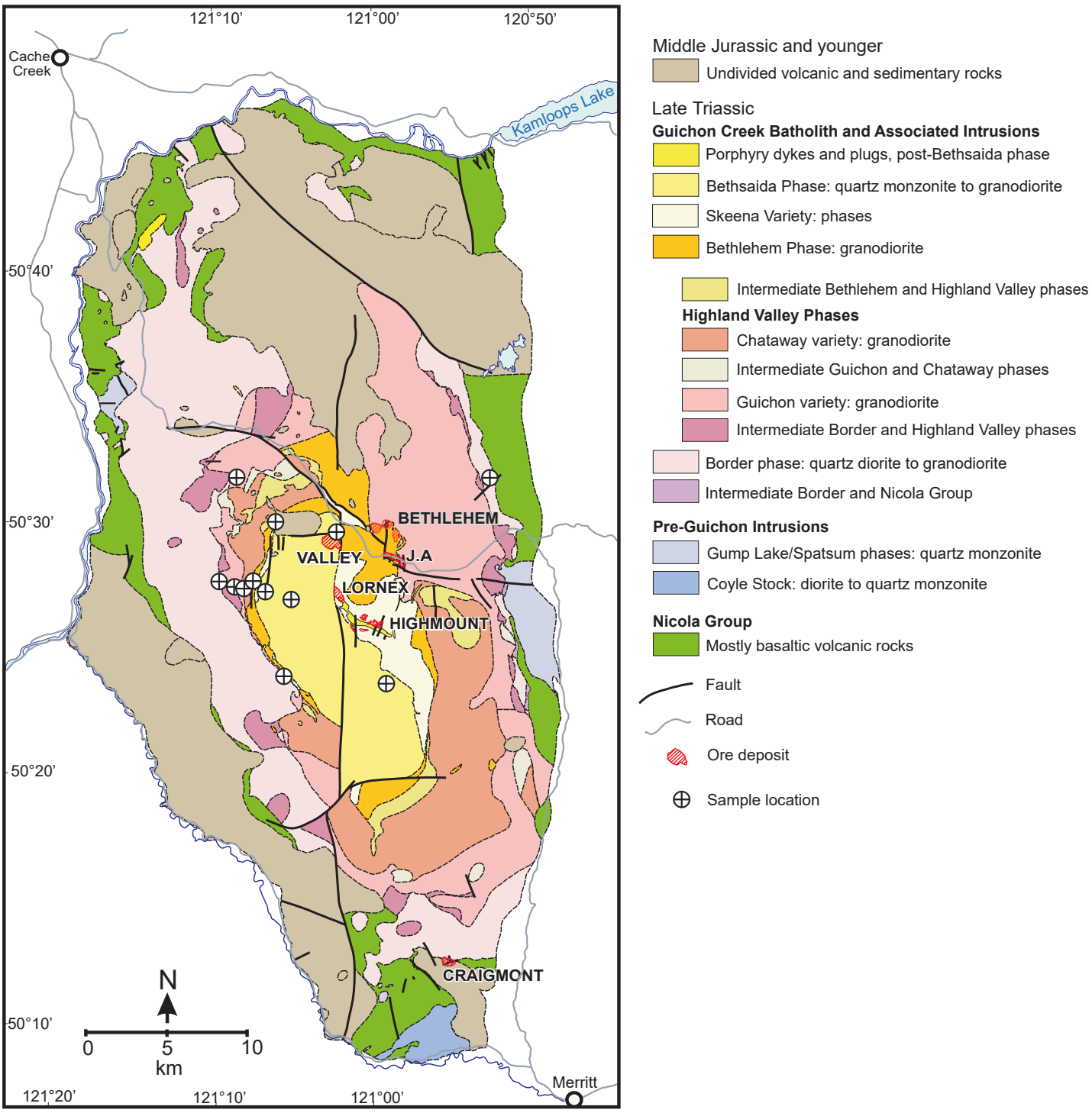

Figure 2: Simplified geology of the Guichon Creek batholith, showing the main intrusive phases, mineral deposits and sample locations (summarized and redrafted after McMillan et al., 2009).

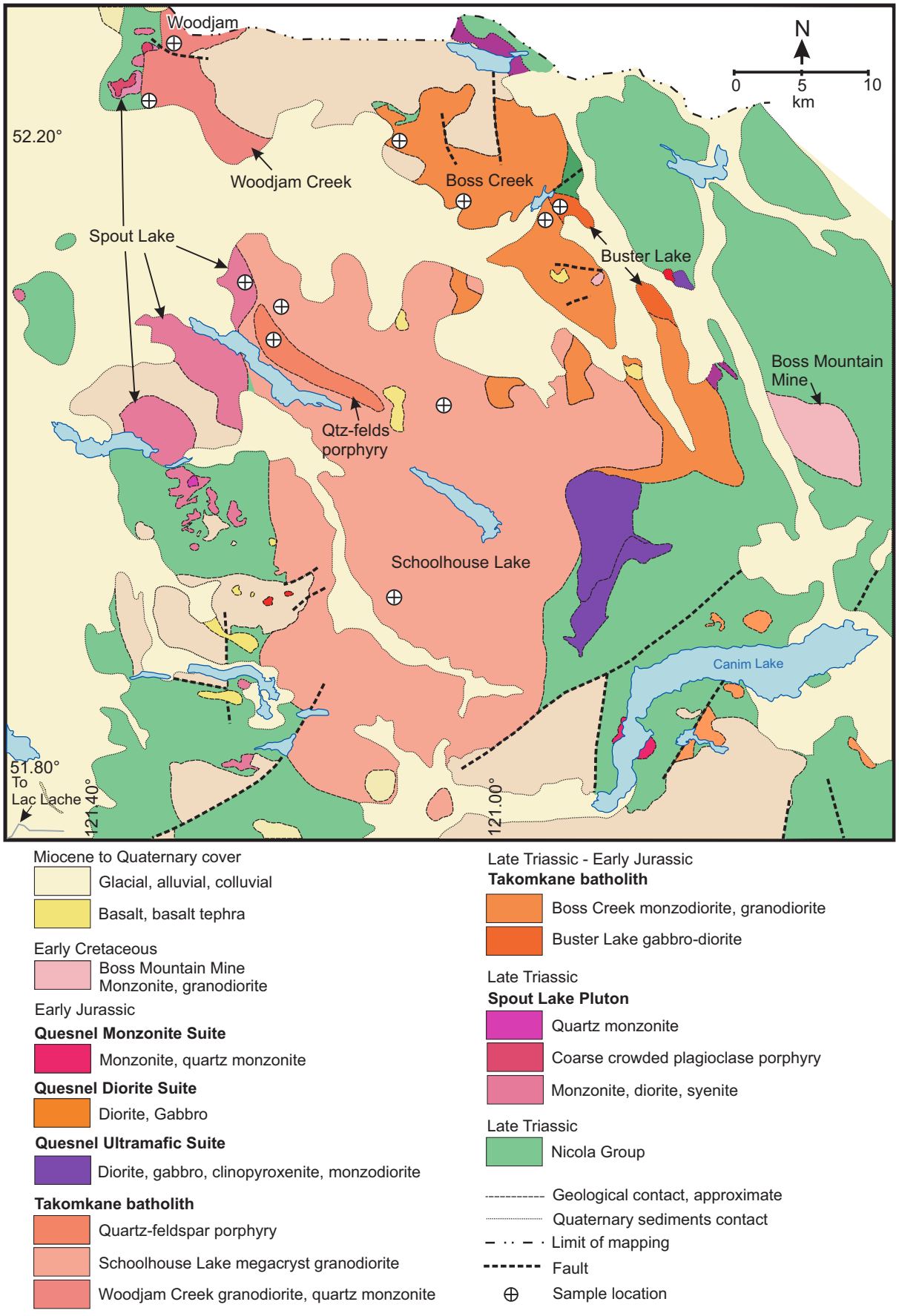

Figure 3: Simplified geology of the Takomkane batholith, showing the main intrusive units and sample locations (after Schiarizza et al., 2013).

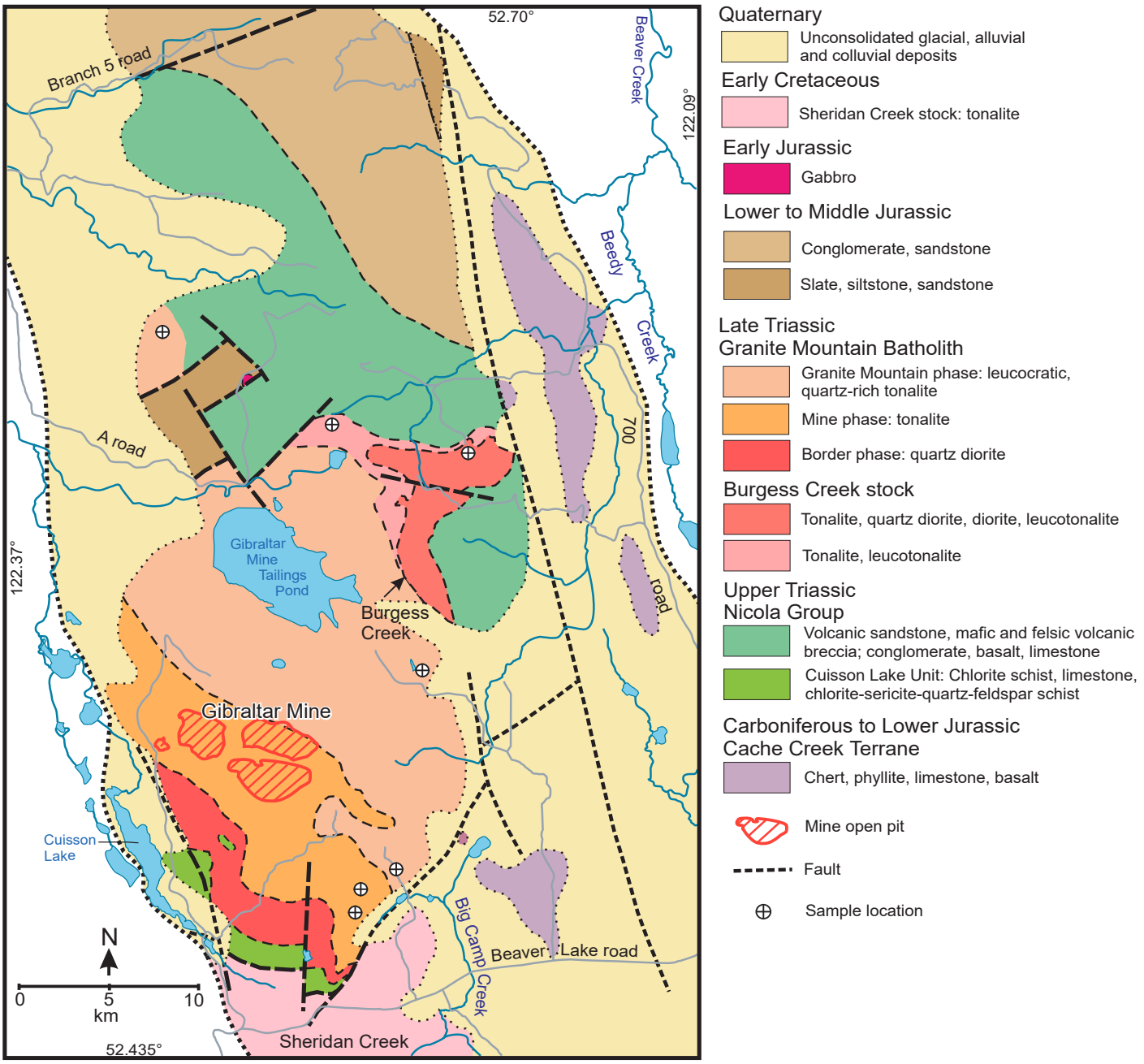

Figure 4: Geology map of the Granite Mountain batholith, showing the main intrusive units and sample locations (after Schiarizza, 2015).

phase-related event that formed the Bethlehem area deposits, and the subsequent Valley, Lornex and Highmont deposit-forming event that occurred in conjunction with the emplacement of the Skeena and Bethsaida phases (Byrne et al., 2013; D'Angelo et al., 2017). Economically, the Valley deposit is an active mine, whereas Lornex and the Bethlehem deposits are past producers, and the Highmont and JA are undeveloped deposits.

3.2 Takomkane Batholith

The Takomkane batholith is a large, 50 x 40 km Late Triassic–Early Jurassic composite batholith 50 km east of Williams Lake that hosts several mineralized porphyry centres. It intrudes the Late Triassic alkaline Spout Lake pluton and is cut by Early Jurassic ultramafic–mafic plutons and the Early Cretaceous Boss Mountain Mine stock (Fig. 3). The Takomkane batholith consists of two major units: the Late Triassic–Early Jurassic Boss Creek unit (202.5 ± 0.5–199.5 ± 0.3 Ma) and the Early Jurassic megacrystic Schoolhouse Lake unit (195.0 ± 0.4–193.5 ± 0.6 Ma) (Schiarizza et al., 2009). A smaller-volume unit of quartz-feldspar porphyry occurs within the Schoolhouse Lake unit. The Woodjam Creek unit (194.99 ± 0.16 Ma, del Real et al., 2017) forms the northwestern part of the batholith (Schiarizza et al., 2009). It is texturally distinct but compositionally similar to the coeval Schoolhouse Lake unit but has less quartz and lacks the characteristic large K-feldspar megacrysts.

Copper mineralization occurs within the Spout Lake pluton and, to a lesser extent, within the Boss Creek and Schoolhouse units (Schiarizza et al., 2009). Mineralization in the Spout Lake pluton consists of occurrences described at Celo, Bory, Murphy Lake, SL, Rover, and Harrison Creek (Schiarizza et al., 2009). These are mostly chalcopyrite, pyrite and locally bornite and magnetite veins. Similar mineralization occurs with the Boss Creek pluton at Rodeo and Lucky Jack prospects. Mineralization within the Schoolhouse Lake pluton occurs at the Granite Mountain prospect in the central parts of the batholith which is characterized by chalcopyrite and pyrite in shear zone hosted quartz veins suggesting a significantly deeper setting for this style of mineralization. The most economically significant Cu-Mo-Au porphyry mineralization occurs along the northwestern boundary of the batholith in the Woodjam area (including the Southeast Zone, Deerhorn and Takom undeveloped deposits). These deposits are hosted within a largely equigranular quartz monzonite unit, for example at Southeast Zone, or in small porphyry dikes and adjacent volcanic rocks, for example at Deerhorn (del Real et al., 2017). Age relationships demonstrate that the Southeast Zone (197.48 ± 0.33 Ma), Takom (197.16 ± 0.15 Ma), and Deerhorn (196.34 ± 0.19 Ma) intrusions were all emplaced over an approximately one million year period as spatially discrete intrusive events (del Real et al., 2017) prior to emplacement of the Schoolhouse units (195.0 ± 0.4 Ma, Schiarizza et al., 2009). The Woodjam Creek unit comprises the margin of the Takomkane batholith. Its coarse-grained textures, geochemical and age similarities with the other mineralized centers suggest that it probably represents a deeper emplaced intrusive stock (del Real et al., 2017).

3.3 Granite Mountain Batholith

The Late Triassic Granite Mountain batholith is 18 x 10 km and occurs 60 km north of Williams Lake near McLeese Lake in south-central BC and hosts the Gibraltar porphyry Cu-Mo mine (Fig. 4). The batholith consists of three main phases, from southwest to northeast: Border phase diorite to quartz diorite, Mine phase tonalite and Granite Mountain phase leucocratic tonalite. The Burgess Creek stock (Panteleyev, 1978), to the northeast, comprises a heterogeneous assemblage of tonalite, quartz diorite and diorite that intrudes the Nicola Group. The Granite Mountain phase (217.2 ± 0.2 Ma, Schiarizza, 2015) is older than the Mine phase (216.2 ± 0.2, Mostaghimi, 2016). More recently, Kobylinski et al. (2020) have divided the Granite Mountain batholith into mineralized and barren phases. The barren phase is the oldest phase with average age of 229.2 ± 4.4 Ma (226.8 ± 8.3 Ma–232 ± 11 Ma) whereas the mineralized phase has been divided into three separate phases dated at 218.9 ± 3.1 Ma, 213.2 ± 2.4 Ma and 205.8 ± 2.1 Ma (Kobylinski et al., 2020). Dating of the Burgess Creek stock shows that it is 4 to 5 m.y. older than the adjacent Granite Mountain phase of the batholith (Schiarizza, 2015) suggesting that the Burgess Creek stock may represent the border phase part of the batholith (Ash et al., 1999).

The Granite Mountain batholith was originally considered to intrude the Cache Creek terrane (Bysouth et al., 1995), but mapping by Schiarizza (2015) convincingly showed Nicola Group strata on the northeastern margin of the Granite Mountain batholith, thus indicating it is part of the Quesnel terrane. Interpretations of aeromagnetic data confirm these observations (Sánchez et al., 2015). Thus, the Granite Mountain batholith is recognized as correlative with the Late Triassic, calc-alkaline Guichon Creek batholith, which hosts the Highland Valley porphyry Cu-Mo deposits, 250 km to the south-southeast.

Mineralization at the Gibraltar mine is hosted in the Mine phase tonalite of the Granite Mountain batholith, but small porphyry-style mineral occurrences are also known in the Border phase and the Granite Mountain phase (Schiarizza, 2015). The Mine phase is typically altered whereas the Border phase and the Granite Mountain phase are rarely altered. Moreover, the age of the mineralization (215 ± 1.0–210 ± 0.5 Ma) based on three Re-Os dates (Harding, 2012) indicates that the mineralization was penecontemporaneous with the emplacement of at least three pulses of the Mine phase (Kobylinski et al., 2020).

3.4 Toodoggone District Plutons

The Toodoggone district (NTS 094E) in northeastern British Columbia, approximately 70 km southeast of Dease Lake, is a 35 x 17 km, NW-trending mineral district located in the eastern Stikine terrane (Fig. 5). Volcanic and sedimentary strata of the Early and Middle Jurassic Hazelton Group underlie much of the Toodoggone district and occupy an elongated structural depression underlain by Late Triassic Takla Group volcanic rocks and less-exposed Permian Asitka Group carbonate units. Clastic sedimentary rocks of the Middle Jurassic to Cretaceous Bowser Lake Group occur to the west and southwest of the Toodoggone district (Diakow, 1990; Diakow et al., 1993, 2005). The Bowser Lake Group sediments, and the younger Sustut Group piggyback basin, were deposited above and protected the Toodoggone district rocks from erosion until their subsequent unroofing. The stratigraphic succession, from oldest to youngest, includes: the Asitka Group, Takla Group, Hazelton Group and the Sustut Group. The Toodoggone Formation rocks are equivalent to the Telkwa Formation of the Hazelton Group (Diakow et al., 1991).

Porphyritic plutons and sub-volcanic stocks intrude the Toodoggone Formation strata. These intrusions are well-exposed in the southern and eastern regions but are presumably barely unroofed in the western and central parts of the district (Diakow et al., 1993). These Early Jurassic granitoid bodies, designated as the Black Lake Plutonic Suite (Woodsworth et al., 1988) form part of an arcuate belt of Late Triassic and Early to Middle Jurassic stocks and composite batholiths that are exposed intermit-

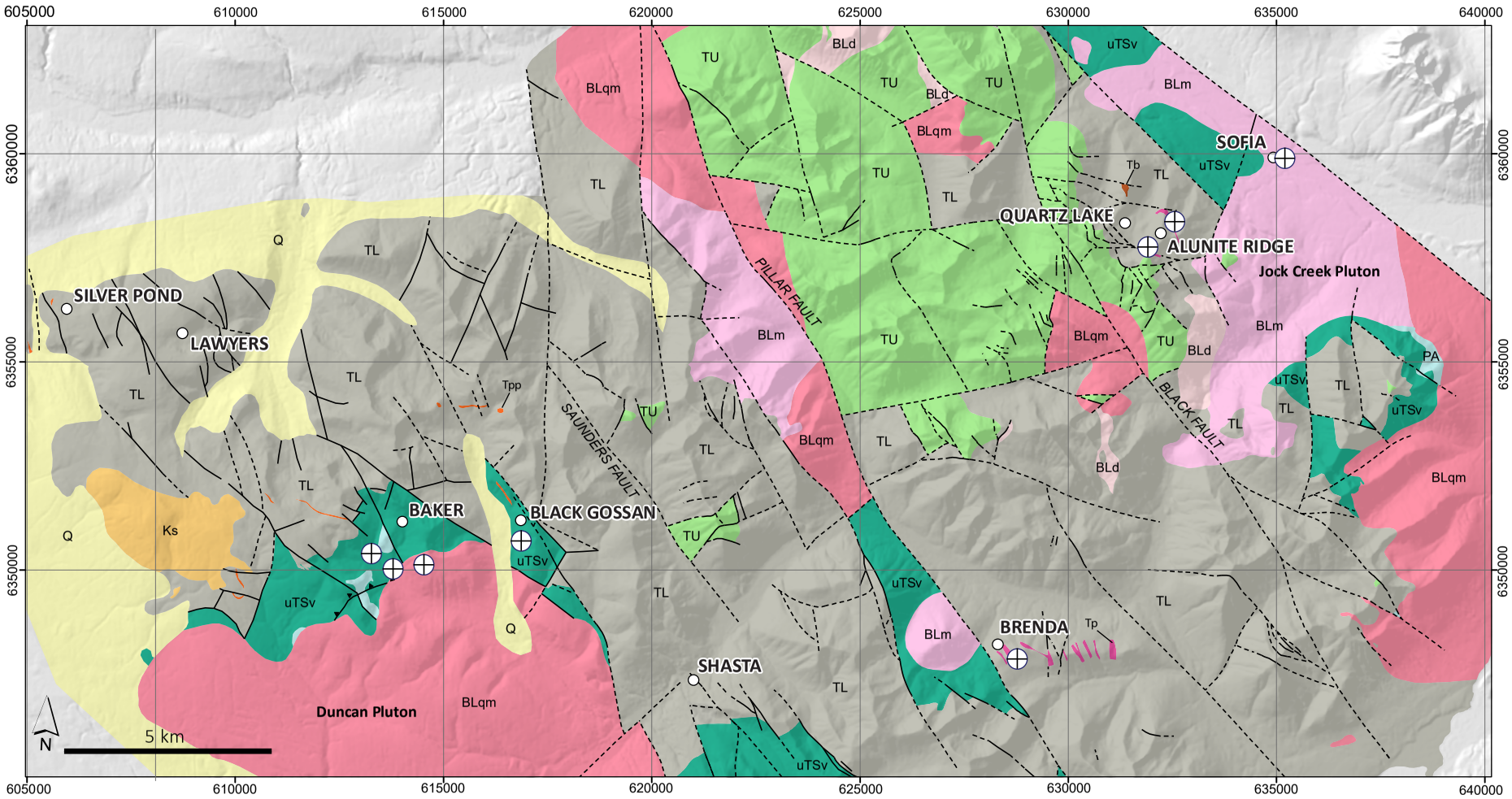

Fault
Mineral Prospect
Sample location

QUATERNARY
Q Sediments

UPPER CRETACEOUS
Ks Conglomerate

LOWER JURASSIC
TU Upper Toodoggone Fm.
TL Lower Toodoggone Fm.

UPPER TRIASSIC
uTSv Takla basalt

PERMIAN
PA Asitka limestone

EARLY JURASSIC INTRUSIVE ROCKS
Tp Tp- Plagioclase porphyry
Tpp Tpp- Pyroxene-plag. porphyry
Tb Tb- Basalt

BLACK LAKE PLUTONIC SUITES
BLd BLd- diorite
BLqm BLqm- Quartz-monzonite
BLm BLm- Monzonite

Figure 5: Geology map of the central Toodoggone district, showing main intrusive units and sample locations (after Diakow et al., 1993, 2005; from Bouzari et al., 2019).

tently along the eastern margin of the Bowser Basin. The Black Lake pluton is a pink granodiorite and quartz monzonite with coarse to medium-grained phenocrysts of plagioclase, orthoclase, quartz, hornblende and biotite. The Giegerich and Jock Creek (196.7 ± 0.3 Ma, Diakow, 2006) plutons occur on the eastern margin of the district and the Duncan Hill pluton (197.9 ± 1.8 Ma, Bouzari et al., 2019) occurs in the western and central parts of the area.

The region is best known for its epithermal Au-Ag deposits (e.g., Lawyers, Shasta, Baker) but also hosts porphyry copper mineralization (Bouzari et al., 2019). Kemess is the major porphyry copper-gold deposit in the district and is associated with the small Maple Leaf (199.6 ± 0.6 Ma, Mortensen et al., 1995) granodiorite pluton (Duuring et al., 2009). Small, and probably deeply eroded, porphyry copper mineralization at the Sofia prospect occurs within the Jock Creek pluton. Several smaller and presumably less eroded plutons, such as the Sovereign pluton near the Kemess deposit or those near the Brenda prospect, occur in the central part of the area.

4. SAMPLES AND METHODS

A total of 127 rock samples were collected from select intrusive phases at each locality. Hand-sawn samples were described and thin sections studied using a petrographic microscope. A subset of 42 samples, representing main intrusive bodies, were selected for zircon separation and analysis, including 12 from the Guichon Creek, 11 from the Takomkane and 6 from the Granite Mountain batholiths, and 13 from the Toodoggone area. The locations of these samples are shown on Figures 2–5 and their descriptions are summarized in Table 1.

Samples were crushed using a Spark 2 electric-pulse disaggregator at Overburden Drilling Management Limited (Nepean, Ontario) to preferentially break the rock along mineral-grain boundaries, thus providing a larger number of unbroken mineral grains. Subsequently, mineral separation was performed at the MDRU-Mineral Deposit Research Unit, The University of British Columbia, using Frantz® magnetic separation and conventional heavy-liquid methods.

Table 1: Samples from the Granite Mountain and Guichon Creek areas selected for analysis. Datum is WGS 84.

Sample#	Latitude	Longitude	Batholith / Area	Unit	Rock type	Description
13PSC-144	52.59492	-122.23555	Granite Mountain	Burgess Creek	leucocratic tonalite	coarse-grained with plagioclase and quartz, hornblende partly altered to chlorite
15Fb-40	52.58959	-122.18362	Granite Mountain	Burgess Creek mixed unit	tonalite	medium-grained, equigranular texture with fresh hornblende and abundant plagioclase
15FB-41	52.52951	-122.19940	Granite Mountain	Granite Mountain	leucocratic tonalite	coarse-grained with equigranular texture with fresh plagioclase and hornblende
15FB-44	52.47754	-122.21181	Granite Mountain	Granite Mountain	leucocratic tonalite	coarse-grained with abundant plagioclase and hornblende altered to chlorite, some quartz
15Fb-43	52.46574	-122.23056	Granite Mountain	Mine phase	tonalite	coarse-grained with weak chlorite alteration, abundant plagioclase and hornblende
15FB-45	52.47221	-122.22703	Granite Mountain	Mine phase	tonalite	coarse grained with large chlorite alteredhornblende and plagioclase
2238895	50.49782	-121.11262	Guichon Creek	Bethlehem phase	granodiorite	coarse-grained with plagioclase, biotite and hornblende
2238791	50.44327	-121.09645	Guichon Creek	Bethsaida Phase	granodiorite	coarse-grained with rounded quartz, plagioclase, biotite and hornblende
09FB-04	50.48893	-121.04612	Guichon Creek	Bethsaida phase	granodiorite	coarse-grained with rounded quartz, plagioclase, pervasive K-feldspar alteration
15FB-08	50.39096	-120.98263	Guichon Creek	Bethsaida phase	granodiorite	coarse-grained with rounded quartz, plagioclase, biotite and hornblende
2238842	50.45516	-121.16772	Guichon Creek	Border phase	granodiorite	coarse-grained with abundant hornblende and plagioclase, local chlorite alteration
2238923	50.52728	-121.15450	Guichon Creek	Border phase	granodiorite	medium-grained with abundant plagioclase and hornblende altered to chlorite
15FB-09	50.52579	-120.88048	Guichon Creek	Border phase	quartz diorite	medium-grained, equigranular with abundant plagioclase and hornblende
2238840	50.45164	-121.15509	Guichon Creek	Border-Guichon phase	granodiorite	coarse-grained with abundant fresh hornblende and plagioclase
2238828	50.45550	-121.13577	Guichon Creek	Chataway variety	granodiorite	coarse-grained with abundant fresh hornblende and plagioclase
2238825	50.45050	-121.14538	Guichon Creek	Guichon variety	granodiorite	coarse-grained with abundant fresh hornblende and plagioclase
15FB-25	50.39412	-121.08642	Guichon Creek	Guichon variety	granodiorite	coarse-grained with plagioclase and hornblende, weak chlorite alteration
2238818	50.44845	-121.12319	Guichon Creek	Skeena variety	granodiorite	coarse-grained, equigranular texture, fresh hornblende, plagioclase

Table 1, cont: Samples from the Takomkane and Toodoggone areas selected for analysis. Datum is WGS 84.

Sample#	Latitude	Longitude	Batholith / Area	Unit	Rock type	Description
15FB-29	52.14648	-121.02687	Takomkane	Boss Creek unit	monzodiorite	coarse-grained equigranular with abundant plagioclase, hornblende and quartz
15FB-31	52.18512	-121.11021	Takomkane	Boss Creek unit	monzodiorite	fine-grained with abundant mafic and grey plagioclase
15FB-34	52.14614	-120.95094	Takomkane	Boss Creek unit	monzodiorite	coarse-grained with grey plagioclase and hornblende
15FB-33	52.15144	-120.93864	Takomkane	Buster Lake unit	gabbro	medium-grained with abundant oriented hornblende
15FB-35	52.06296	-121.23232	Takomkane	Quartz-feldspar porphyry	quartz feldspar porphyry	coarse-grained with abundant creamy plagioclase and rounded quartz
15FB-36	52.07690	-121.21588	Takomkane	Schoolhouse Lake unit	granodiorite	coarse-grained with abundant plagioclase, K-feldspar and quartz
15Fb-37	52.01909	-121.05282	Takomkane	Schoolhouse Lake unit	granodiorite	coarse-grained with abundant plagioclase, K-feldspar and quartz
15FB-38	51.90980	-121.09556	Takomkane	Schoolhouse Lake unit	granodiorite	coarse-grained with abundant plagioclase, K-feldspar and quartz
15FB-28	52.09534	-121.25233	Takomkane	Spout Lake pluton	monzodiorite	coarse-grained equigranular with abundant plagioclase and hornblende
10FB-01	52.22165	-121.36176	Takomkane	Woodjam Creek	quartz monzonite	coarse-grained equigranular with plagioclase, biotite, hornblende and quartz
11FB-01	52.25747	-121.34199	Takomkane	Woodjam Creek	quartz monzonite	coarse-grained equigranular with plagioclase, biotite, hornblende and quartz
16FB-11	57.34409	-126.80707	Toodoggone	Alunite Ridge	granodiorite	coarse-grained, equigranular with grey plagioclase, pink K-feldspar, hornblende
16FB-12	57.34813	-126.80232	Toodoggone	Alunite Ridge	syenite	fine-grained, pink K-feldspar-rich
16FB-10	57.27540	-127.12509	Toodoggone	Baker skarn dike	monzogranite	medium-grained with K-feldspar and pyroxene
16FB-09	57.27354	-127.11803	Toodoggone	Baker skarn pluton	monzogranite	coarse-grained with plagioclase, K-feldspar, biotite and hornblende
16FB-04	57.28321	-127.06484	Toodoggone	Black Gossan	monzonite	coarse-grained monzonite porphyry with abundant K-feldspar
16FB-15			Toodoggone	Black Lake mineralized	monzonite	porphyry texture with plagioclase and hornblende in fine, green groundmass (from drill hole KH-14-04 at
16FB-06	57.25537	-126.87157	Toodoggone	Brenda syenite dike	syenite	medium-grained with abundant K-feldspar and some epidote alteration
16FB-03	57.17791	-127.03520	Toodoggone	Duncan pluton	granodiorite	coarse-grained equigranular with plagioclase, biotite, hornblende and K-feldspar alteration
16FB-05	57.27311	-127.10072	Toodoggone	Duncan pluton	granodiorite	coarse-grained with plagioclase, hornblende, biotite and K-feldspar
16FB-16			Toodoggone	Kemess post mineral dyke	feldspar porphyry	coarse-grained porphyry texture with plagioclase, biotite, quartz (from KH-14-04 at 980 m)
16FB-13	57.36287	-126.75617	Toodoggone	Sofia	granodiorite	coarse-grained with abundant pink K-feldspar and some magnetite alteration
16FB-14	57.36287	-126.75613	Toodoggone	Sofia	mafic phase?	fine-grained mafic phase or body
16FB-17			Toodoggone	Sovereign pluton	granodiorite	coarse-grained with fresh plagioclase, hornblende (from KH-07-01A at 657)

Mineral grains were handpicked, mounted and polished in preparation for electron-probe microanalysis (EPMA) and trace-element laser-ablation inductively coupled plasma-mass spectrometry (LA-ICP-MS) at the Pacific Centre for Isotopic and Geochemical Research (PCIGR), University of British Columbia. A total of 1021 zircon grains were mounted and analyzed. These grains were studied and characterized by binocular, petrographic and CL microscopy. Properties such as colour, shape, inclusion populations and zoning were documented for each grain. Mineral grains and spots were then analyzed by EPMA for major elements and some trace elements before being analyzed by LA-ICP-MS for a full trace-element characterization. A total of 1620 spots were analyzed by EMPA of which 1397 spots were analyzed by ICP-MS. Some spots analyzed by EPMA were too small for ICP-MS analyses. In the case of smaller grains (<100 µm), one spot was analyzed per sample, whereas for larger grains (>100 µm), two spots were analyzed per grain, one at the grain centre and one at the rim.

Table 2: Geochemical results for the Guichon Creek and Takomkane samples.

Batholith	**Guichon Creek**					**Takomkane**					
Unit	Bethsaida	Bethlehem	Skeena	Chataway	Border	Woodjam Creek	Qtz-feldspar porphyry	Schoolhouse Lake	Boss Creek	Buster Lake	Spout Lake
Rock type	granodiorite	granodiorite	granodiorite	granodiorite	granodiorite	qtz monzonite	QF porphyry	granodiorite	monzodiorite	gabbro	monzodiorite
Sample#	2238791	2238895	2238818	2238828	2238923	10FB-01	15FB-35	15FB-38	15FB-34	15FB-33	15FB-28
Analysis#	P12-06-8	P12-04-17-1	P01-11-11	P12-08-3-2	P12-03-2	P12-01-3-2	P01-03-9	P02-06-20-1	P01-07-19	P01-02-12	P02-04-9
Zoning	concentric	concentric	concentric	tabular-concen.	concentric	concentric	concentric	concentric	tabular	concentric	tabular
Texture	regular	crossed	regular	regular	regular	regular	regular	regular	irregular	regular	regular
Electron-probe microanalysis (wt.%):											
Si	31.13	31.20	32.39	31.74	31.03	31.49	32.39	32.04	31.95	32.40	32.18
Zr	67.02	66.67	67.99	66.37	65.42	65.33	64.63	67.21	65.88	64.91	66.94
Hf	1.60	1.46	1.50	1.55	1.41	1.39	1.56	1.65	1.14	1.27	1.18
U	0.03	0.03	0.05	0.04	0.00	0.04	0.07	0.06	0.21	0.04	0.08
LA-ICP-MS microanalysis (ppm):											
^{7}Li	3.4	<DL	<DL	<DL	<DL	<DL	<DL	2.3	1.8	2.4	0.5
^{31}P	540.0	154.0	780.0	334.0	269.0	209.0	207.0	105.0	<DL	<DL	541.0
^{43}Ca	790.0	80.0	-55.0	<DL	<DL	210.0	50.0	100.0	90.0	1030.0	120.0
^{45}Sc	305.8	325.3	319.2	325.6	340.7	346.5	253.1	263.0	278.5	250.9	285.9
^{49}Ti	17.4	9.4	8.2	11.9	15.0	15.0	3.5	3.6	4.0	5.5	18.0
^{89}Y	404.2	869.0	279.5	818.0	644.4	577.0	649.5	641.0	1350.0	284.0	774.0
^{93}Nb	<DL	<DL	<DL	<DL	0.6	0.5	1.4	0.9	0.9	<DL	0.7
^{139}La	12.5	<DL	<DL	<DL	<DL	<DL	<DL	<DL	<DL	<DL	<DL
^{140}Ce	28.6	11.8	6.4	9.0	12.9	6.0	14.2	17.3	4.5	2.5	4.8
^{141}Pr	2.0	0.2	<DL	<DL	<DL	<DL	<DL	<DL	<DL	<DL	<DL
^{146}Nd	7.4	2.8	0.3	2.0	1.1	<DL	<DL	<DL	1.1	<DL	1.5
^{147}Sm	2.1	5.0	0.9	4.7	3.3	1.0	0.8	0.9	3.2	0.3	2.6
^{153}Eu	0.8	1.2	<DL	1.1	<DL	0.5	<DL	0.5	0.5	<DL	0.6
^{157}Gd	8.1	21.9	4.4	18.9	14.8	9.4	6.8	6.1	19.2	2.9	13.9
^{159}Tb	2.3	6.4	1.6	5.9	4.5	3.3	2.6	2.4	7.9	1.3	4.7
^{163}Dy	31.4	73.3	20.8	75.5	56.8	43.9	41.7	35.9	107.9	18.2	64.5
^{165}Ho	12.3	27.6	8.5	25.4	21.6	18.4	19.2	17.4	44.9	8.3	24.6
^{166}Er	64.5	132.3	44.6	117.1	105.4	95.7	110.8	106.1	232.0	48.7	127.0
^{169}Tm	14.2	30.7	11.7	23.5	21.4	24.8	29.4	29.0	52.4	12.5	29.1
^{172}Yb	156.5	309.7	127.3	212.9	210.6	275.0	328.4	339.0	525.0	138.2	278.0
^{175}Lu	34.9	65.1	31.0	39.9	43.5	63.5	86.3	94.6	106.9	34.8	60.8
^{177}Hf	9025.0	9151.0	10026.0	8060.0	10740.0	10143.0	10140.0	12180.0	10660.0	9497.0	9880.0
^{204}Pb	<DL	1.1	6.0	<DL	1.1	<DL	24.0	5.0	3.8	9.0	1.4
^{206}Pb	18.3	10.0	6.0	10.5	23.7	10.3	46.8	62.9	51.6	33.8	15.2
^{207}Pb	3.9	0.5	<DL	0.8	1.2	<DL	2.6	3.7	3.1	2.0	0.8
^{208}Pb	4.1	0.8	<DL	1.1	1.5	<DL	2.7	6.0	2.3	1.2	1.0
^{232}Th	67.5	40.0	15.7	50.5	83.0	24.5	135.6	353.0	116.0	59.5	49.1
^{235}U	392.0	213.0	145.0	245.0	592.0	195.0	1102.0	1628.0	1380.0	858.0	358.0
^{238}U	108.3	72.5	45.1	72.6	162.2	87.6	357.5	522.0	391.0	255.0	111.4
Ti-in-Zircon T (°C)	801	740	728	763	786	786	656	658	667	693	804
Eu Anomaly	0.63	0.35	0.60	0.35	0.20	0.45	0.58	0.65	0.21	0.31	0.28

Table 2, cont: Geochemical results for the Granite Mountain and Toodoggone samples.

Batholith	Granite Mountain				Toodoggone								
Unit	Mine phase	Granite Mountain	Burgess Creek mixed	Burgess Creek	Black Lake Mineralized	Sofia	Dunkan (Kemess)	Sovereign	Duncan (Baker Skarn)	Duncan (Black Gossan)	Brenda dike	Alunite Ridge dyke	Kemess dyke
Rock type	tonalite	tonalite	tonalite	tonalite	monzonite	granodiorite	granodiorite	granodiorite	granodiorite	monzonite	syenite	monzonite	felds. porphyry
Sample#	15Fb-43	15FB-44	15Fb-40	13PSC-144	FB16-15	FB16-13	16FB-05	16FB-17	16FB-09	FB16-04	16FB-06	FB-16-11	16FB-16
Analysis#	P01-06-15-1	P01-01-4	P01-08-24	P12-10-7-2	P28-06-12	P28-02-5-2	P24-02-5-1	P24-03-18-1	P24-04-1-1	P28-04-8-2	P24-07-8-2	P28-03-3-2	P24-01-12-2
Zoning	tabular-concen.	concentric	concentric	concentric	concentric	concentric	concentric	concentric	concentric	concentric	tabular-concen.	concentric	concentric
Texture	irregular	crossed	regular	regular	regular	regular	regular	regular	regular	regular	crossed	regular	regular
Electron-probe microanalysis (wt.%):													
Si	31.94	32.41	32.33	31.71	32.37	31.79	31.70	31.92	32.49	32.18	32.52	32.42	32.72
Zr	65.44	65.87	67.52	66.61	66.90	67.41	67.09	66.55	67.63	66.81	67.02	67.21	66.14
Hf	1.35	1.27	1.38	1.67	1.50	1.47	1.38	1.41	1.28	1.30	1.21	1.30	1.20
U	0.07	0.03	0.03	0.08	0.07	0.11	0.04	0.11	0.14	0.08	0.06	0.08	0.07
LA-ICP-MS microanalysis (ppm):													
^{7}Li	<DL	<DL	8.2	5.9	<DL	<DL	<DL	<DL	<DL	<DL	<DL	<DL	<DL
^{31}P	331.0	944.0	350.0	309.0	105.0	194.0	272.0	215.0	91.0	30.0	<DL	1000.0	188.0
^{43}Ca	160.0	15.0	70.0	<DL	<DL	<DL	<DL	150.0	<DL	<DL	240.0	<DL	<DL
^{45}Sc	273.0	429.7	365.1	351.3	208.1	175.2	221.9	218.5	192.8	183.0	188.7	228.0	227.2
^{49}Ti	17.8	4.7	17.4	2.3	<DL	8.5	6.0	3.3	3.0	7.0	3.4	5.7	4.9
^{89}Y	925.6	943.0	1600.0	682.0	822.0	597.0	775.0	867.0	369.0	341.0	860.0	1136.0	406.0
^{93}Nb	<DL	0.9	1.2	0.9	0.7	1.4	2.3	2.6	1.4	0.7	1.4	2.8	0.8
^{139}La	<DL	<DL	<DL	<DL	< <DL	<DL	<DL	<DL	<DL	<DL	<DL	<DL	<DL
^{140}Ce	5.8	8.1	10.5	9.3	10.6	11.0	13.0	19.5	10.8	7.3	11.9	18.8	6.5
^{141}Pr	<DL	<DL	<DL	<DL	< <DL	<DL	<DL	<DL	<DL	<DL	<DL	<DL	<DL
^{146}Nd	1.3	0.5	1.9	<DL	1.0	<DL	0.8	0.9	0.2	<DL	1.1	0.8	<DL
^{147}Sm	3.3	1.9	4.1	1.2	2.4	0.9	1.3	2.2	0.9	0.7	2.5	2.3	0.9
^{153}Eu	0.6	0.5	1.0	<DL	1.3	0.5	0.5	0.9	<DL	<DL	0.9	0.7	0.5
^{157}Gd	19.4	12.9	25.7	7.6	13.6	6.9	10.3	11.8	5.7	4.0	11.2	16.5	4.6
^{159}Tb	6.4	5.0	9.6	3.1	4.3	2.8	4.0	4.3	1.8	1.6	4.3	5.5	1.8
^{163}Dy	82.3	72.0	129.6	44.8	60.7	38.3	55.5	61.4	25.6	23.8	64.2	82.0	27.4
^{165}Ho	30.4	30.0	50.0	19.5	25.3	17.9	24.0	26.5	11.6	10.8	26.5	34.6	12.3
^{166}Er	141.1	164.5	252.4	116.3	138.2	101.2	136.3	143.7	67.5	61.7	152.2	184.6	76.2
^{169}Tm	29.7	38.4	56.1	32.0	33.6	26.2	32.8	37.3	17.6	15.2	38.8	44.4	19.1
^{172}Yb	262.2	391.5	535.0	351.0	370.0	269.0	335.0	384.7	186.8	167.4	388.1	452.0	221.5
^{175}Lu	52.3	89.0	105.7	89.5	86.3	64.6	76.9	91.5	47.3	39.9	93.7	104.1	57.2
^{177}Hf	10458.0	10320.0	11030.0	12870.0	9114.0	8330.0	10035.0	8771.0	9240.0	9142.0	8550.0	8110.0	10140.0
^{204}Pb	<DL	5.5	8.0	6.7	5.2	<DL	<DL	3.3	<DL	11.2	4.5	14.5	3.1
^{206}Pb	6.5	7.1	42.2	32.3	34.6	27.0	44.7	61.0	50.2	20.6	30.0	47.0	16.1
^{207}Pb	0.5	<DL	2.3	1.9	2.3	1.5	2.8	3.6	2.6	1.1	1.8	2.3	1.0
^{208}Pb	0.5	<DL	3.1	0.8	2.1	1.6	2.7	3.9	2.1	1.0	1.6	3.0	0.6
^{232}Th	17.1	12.5	157.6	38.0	103.1	89.0	151.0	210.0	120.0	56.7	108.0	163.0	37.3
^{235}U	116.0	154.0	812.0	740.0	921.0	548.0	1071.0	1590.0	1320.0	881.0	761.0	1740.0	413.0
^{238}U	45.1	50.3	296.6	230.0	276.0	201.0	347.0	441.0	370.0	158.5	256.4	369.0	138.8
Ti-in-Zircon T (°C)	803	680	801	624		731	700	652	644	714	654	696	683
Eu Anomaly	0.23	0.28	0.29	0.29	0.67	0.58	0.42	0.56	0.51	0.59	0.53	0.35	0.76

4.1 Analytical Methods

A Cambridge Image Technology Ltd MK 4A model cold cathodoluminescence (CL) stage mounted on a petrographic microscope was used to study the internal textures of the zircon grains. The samples were irradiated in a vacuum chamber with an electron beam of approximately 15 kV and the current set at 350–500 µA. Petrographic studies of zircon grains under transmitted light and CL were used to select areas free of inclusions for analysis.

Electron-probe microanalyses of zircon was conducted using a fully automated CAMECA SX-50 instrument, operating in the wavelength-dispersion mode with the following operating conditions: excitation voltage, 15 kV; beam current, 20 nA; peak count time for Si and Zr, 20 s; background count-time for Si and Zr, 10 s; peak count time for Hf and U, 100 s; background count-time for Hf and U, 50 s; spot diameter, 5 µm. Data reduction was done using the 'PAP' $\phi(\rho Z)$ method (Pouchou and Pichoir, 1985). For the elements considered, the following standards, X-ray lines and crystals were used: zircon, SiKα, TAP; zircon, ZrLα, PET; Hf metal, HfLα, LIF; UO_2 glass, UMα, PET.

Analyses using LA-ICP-MS were carried out with a Resonetics m50-LR 193 nm Excimer laser coupled to an Agilent 7700x ICP-MS with laser diameter of approximately 34 µm. Ablation time was 40 s with He gas flow (750 ml/min He and 2 ml/min N_2). Thirty-three masses were analyzed, including ^{91}Zr as the internal standard, using the concentrations obtained by EPMA. Glitter 4.0 software was used to determine elemental concentrations using a NIST SRM 612 glass standard for external standardization. Intervals for data reduction were chosen based on the flattest part of the ^{91}Zr plateau, typically ~2 seconds after the laser turned on and ~2 seconds before the laser was turned off. During the data reduction a careful check on the multi-element mass spectra eliminated any possible impurities that may have been encountered across the depth profile of each laser-ablated area by assessing the ^{91}Zr profile and inspecting for depressions, and examining for spikes of other masses that indicated the presence of inclusions. In total, 1397 spots were analyzed from 1021 zircon grains of which 205 spots analyzed were rejected. The precision and accuracy of the analyses undertaken during this study are better than ±10%. Table 2 provides results of chemical analyses of representative zircon grains from each batholith.

5. ZIRCON TEXTURES

Zircon grains in the studied plutons display a great variety of textures. Zircon typically occurs as 100 to 500 µm long grains with complex internal zoning but the grain size does not vary significantly between various plutonic phases. Cathodoluminescence imaging was used to characterize the texture of the zircon grains. Zircon zoning is classified into five types (Fig. 6):

Oscillatory zoning is the most common type of zoning (Fig. 6a), creating zones of green, dark green and grey luminescence. Cyclic zoning of fine (<1–5 µm) to thicker bands (>10 µm) is common and occurs around a larger core with uniform luminescence. Some zircon grains locally have a black luminescent core, with an irregular shape resembling an antecryst. **Tabular zoning** is common in elongate zircon grains (Fig. 6b), which occurs as thick (10–40 µm) parallel bands (ca. 5–8) of green, light green, grey or black coloured luminescence; however, fine parallel zoning is not common. **Tabular-oscillatory zoning** is simply a combination of tabular and oscillatory zones in a single grain (Fig. 6c) and is characterized by tabular zoned zircon cores rimmed by oscillatory zones. However, zircon grains with oscillatory zones rimmed by tabular zones were not observed. The observed relationships suggest that zircons with tabular zoning in each sample always formed prior to the zircons with oscillatory zoning. **Sector zoning** occurs in some zircons that show oscillatory zoning (Fig. 6d). **Irregular zoning** commonly occurs in zircon with oscillatory zoning and is distinctly different; in such grains, new growth zones crosscut older zones (Fig. 6e, f), thus suggesting that new zircon zones formed by modifying (resorbed or recrystallized) or on top of older zones. Similar irregular zoning can be ascribed to some disequilibrium processes during zircon growth (Gagnevin et al., 2010). Geisler et al. (2007) inferred a diffusion-limited dissolution–recrystallization process along a reaction front as a cause for disequilibrium during zircon growth.

6. ZIRCON TRACE-ELEMENT CHEMISTRY

Zircon is a robust mineral that can crystallize from melt over a wide range of magmatic temperatures, depending on the bulk composition of the host magma (Harrison and Watson, 1983). Zircon structure can incorporate many trace elements due to sluggish diffusion for most trace elements in zircon (Cherniak and Watson, 2003). Moreover, because of the slow rates of oxygen diffusion for these elements (Cherniak et al., 1997), zircon retains its initial compositions and provides a record of the magmatic processes that occurred during zircon growth such as crystal fractionation, oxidation state and temperature, all important factors in the formation of porphyry copper deposits (Thomas et al., 2002; Belousova et al., 2006). Zircons in plutonic rocks associated with porphyry copper deposits typically display low abundances of light rare-earth elements (LREE) and high relative abundances of heavy rare-earth elements (HREE), with positive Ce and negative Eu anomalies (Ballard et al., 2002; Dilles et al., 2015). Typically, in mineralized intrusions, the Ce anomaly is larger and the Eu anomaly smaller in magnitude, compared to nonmineralized intrusions (Ballard et al., 2002).

6.1 HREE Enrichment

The Th/U versus Yb/Gd plot shows that zircon composition evolved on a curved path for all batholiths, with Yb/Gd increasing as Th/U decreases (Fig. 7). The Guichon Creek batholith displays a wide range of Th/U and Yb/Gd values for zircons from both barren and mineralized phases (Fig. 7a). However, most

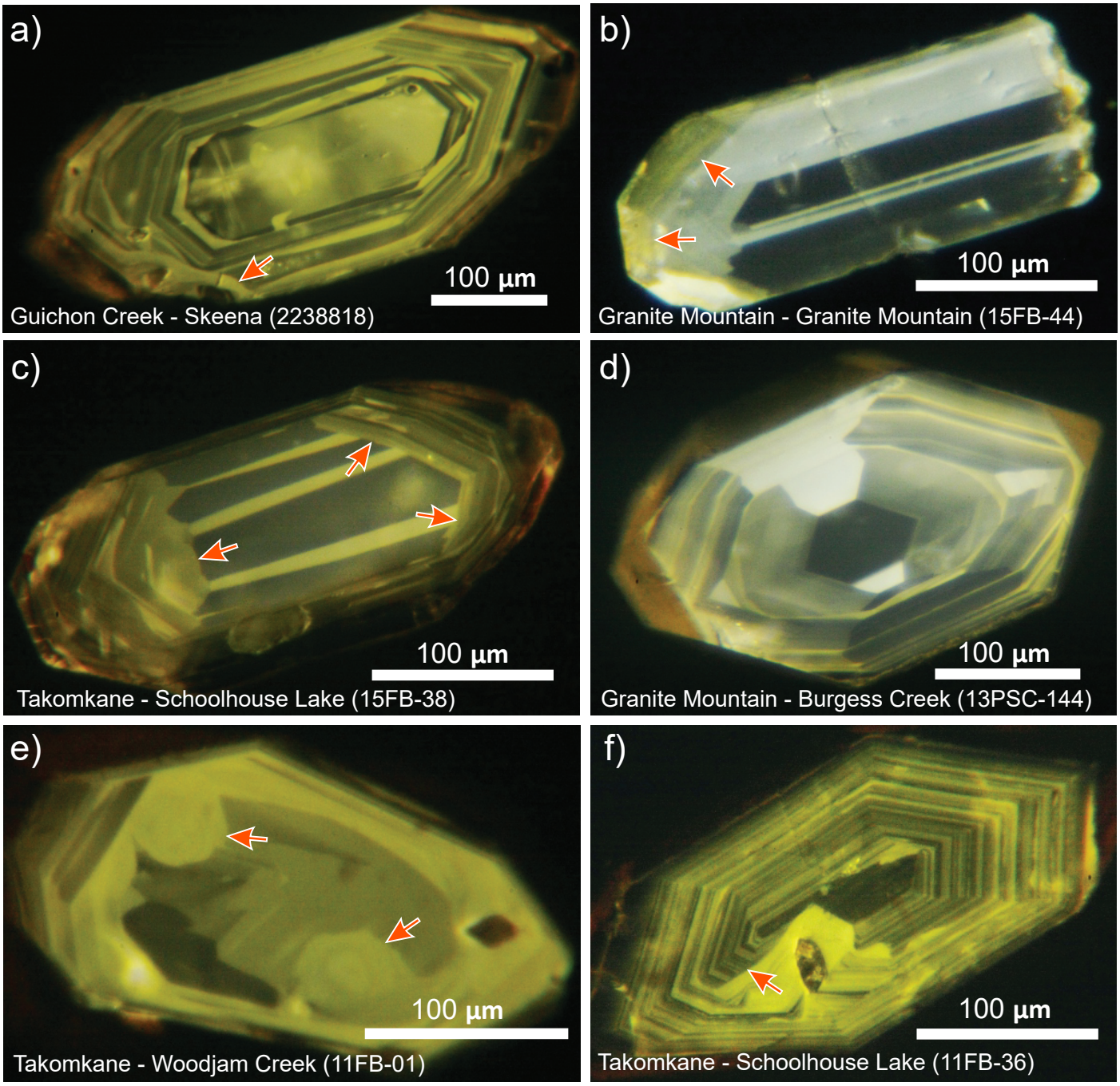

Figure 6: Cathodoluminescence images of zircon grains, showing various types of zoning: a) oscillatory zoning in a zircon grain, with some irregular zoning where younger zones crosscut older zones near the rim (indicated by the arrow); b) tabular zoning, with oscillatory zoning evident near the rim (indicated by the arrows); c) tabular zoning rimmed by oscillatory zoning (indicated by the arrows); d) oscillatory and sector zoning; e) and f) irregular rim zoning impinging on the core zoning (indicated by the arrows). Batholith, pluton and sample number are shown at the bottom of each image.

zircons from the earlier phases, such as the Border and Guichon phases, have high Th/U and low Yb/Gd (>0.45 and <15 respectively), whereas mineralized phases, such as Bethsaida and Skeena, have zircons with lower Th/U and higher Yb/Gd (<0.45 and >15 respectively). Similarly, in the Takomkane batholith area, results from zircons recovered from the older phases (e.g., Spout Lake, Buster Lake and Boss Creek) show a curved path, with a wide range of compositions but with higher Yb/Gd and lower Th/U for the Boss Creek relative to the Spout Lake phase (Fig. 7b). Zircon compositions of the mineralized Woodjam Creek phase, clustered in the middle of the curve, present a range of Yb/Gd and Th/U that are strikingly similar to those of the Bethsaida phase of the Guichon Creek batholith. Zircons from the Schoolhouse Lake and quartz-feldspar porphyry phases of the Takomkane batholith are scattered and largely fall off the main curve (Fig. 7b). The zircons from the Granite Mountain batholith follow a similar curve on Yb/Gd versus Th/U plot (Fig. 7c), with the mineralized Mine phase, which occurs in the middle of

the curve, displaying similar Th/U to those of zircons from the Guichon Creek and Takomkane batholiths (between 0.25 and 0.45) but slightly lower Yb/Gd (>10). Samples from the Toodoggone area show a broad curved path, with overlap of Th/U and Yb/Gd of the various phases (Fig. 7d). Zircons from the mineralized phases at Kemess, especially Black Lake, and Sofia have low Th/U (<0.5) and high Yb/Gd (>20).

6.2 Crystal Fractionation

The decrease in Th/U in zircons is attributed to crystal fractionation producing residual melts with relatively high U and Th contents but low Th/U, because U is strongly portioned into zircon relative to Th (Miller and Wooden, 2004). The Yb/Gd increase is attributed to apatite, hornblende and titanite crystallization: as the magma cools and crystallizes, apatite, hornblende and titanite fractionation preferentially depletes the melt in MREE (mid rare earth elements Sm, Eu, Gd, Tb, Dy, Ho), causing elevated HREE (heavy rare earth elements Er, Tm, Yb, Lu) in zircon relative to MREE, and thus high Yb/Gd. The similarity of Th/U and Yb/Gd in zircons from the mineralized phases suggests that fertile magmas have undergone a certain amount of fractional crystallization. The variation in zircon compositions along the observed evolutionary paths reflects different proportions of apatite, hornblende and titanite in the sequence of crystallization (Lee at al., 2017b). This is more notable for zircons from the Mine phase of the Granite Mountain batholith that have slightly lower Yb/Gd (10–25) relative to the Bethsaida and Woodjam Creek phases, for example (Yb/Gd = 20–40), which suggests less fractionated rock. The distribution pattern of Th/U and Yb/Gd of zircons from the poorly mineralized Schoolhouse Lake and quartz-feldspar porphyry units of the Takomkane batholith is a broad poorly defined curved path suggestive of a crystal fractionation path (Fig. 7b).

Scattering, or poorly defined fractionation paths, are probably due to the melts assimilating U-, Th- and REE-enriched crustal materials during magma evolution. Lee et al. (2017b) came to the same conclusion and suggested that poorly mineralized rocks at El Salvador, in Chile, display evidence of crustal mixing and contamination, whereas the mineralized phases show no evidence of contamination but simple crystal fractionation.

6.3 Eu Anomaly and Oxidation State

The europium anomaly (Eu_N/Eu_N^*) is typically calculated as the ratio of chondrite-normalized Eu abundance relative to Sm and Gd. Europium in magma exists mainly as Eu^{2+}, which preferentially partitions into crystallizing plagioclase feldspars and thus generates a negative Eu anomaly in the residual magma and subsequent crystalizing zircon. Higher oxidation states promote an increase in the abundance of Eu^{3+}, which favours partitioning into zircon and thus decreases the negative Eu anomaly in zircons. Ce^{4+}/Ce^{3+} ratios of zircon are also indicators of oxidation state of the melt but for several reasons measurement of the

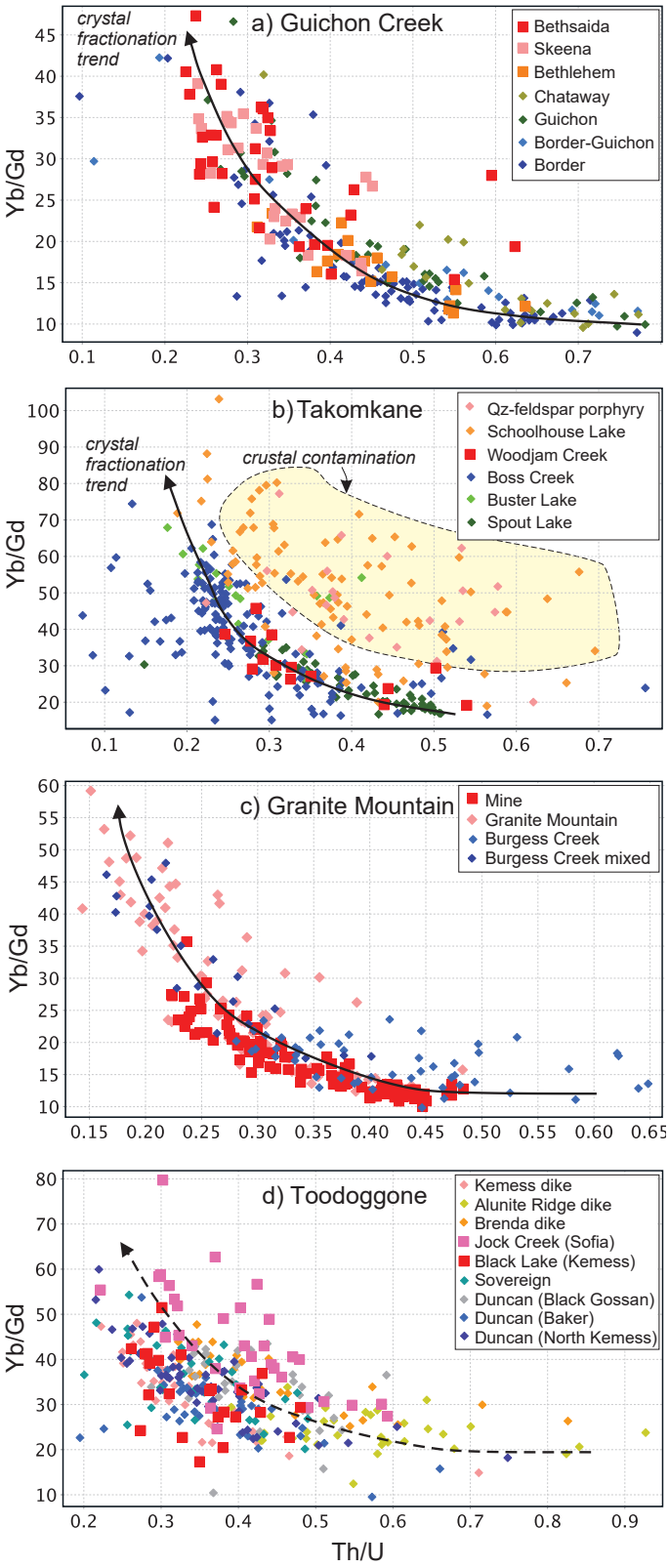

Figure 7: Binary diagram of Th/U versus Yb/Gd, showing the curved evolution path for zircons characterized by moderate to high crystal fractionation and from porphyry-fertile plutons and zircons from unmineralized phases showing scatter plot probably due to crustal contamination a) Guichon Creek batholith; b) Takomkane batholith; c) Granite Mountain batholith; d) Toodoggone area.

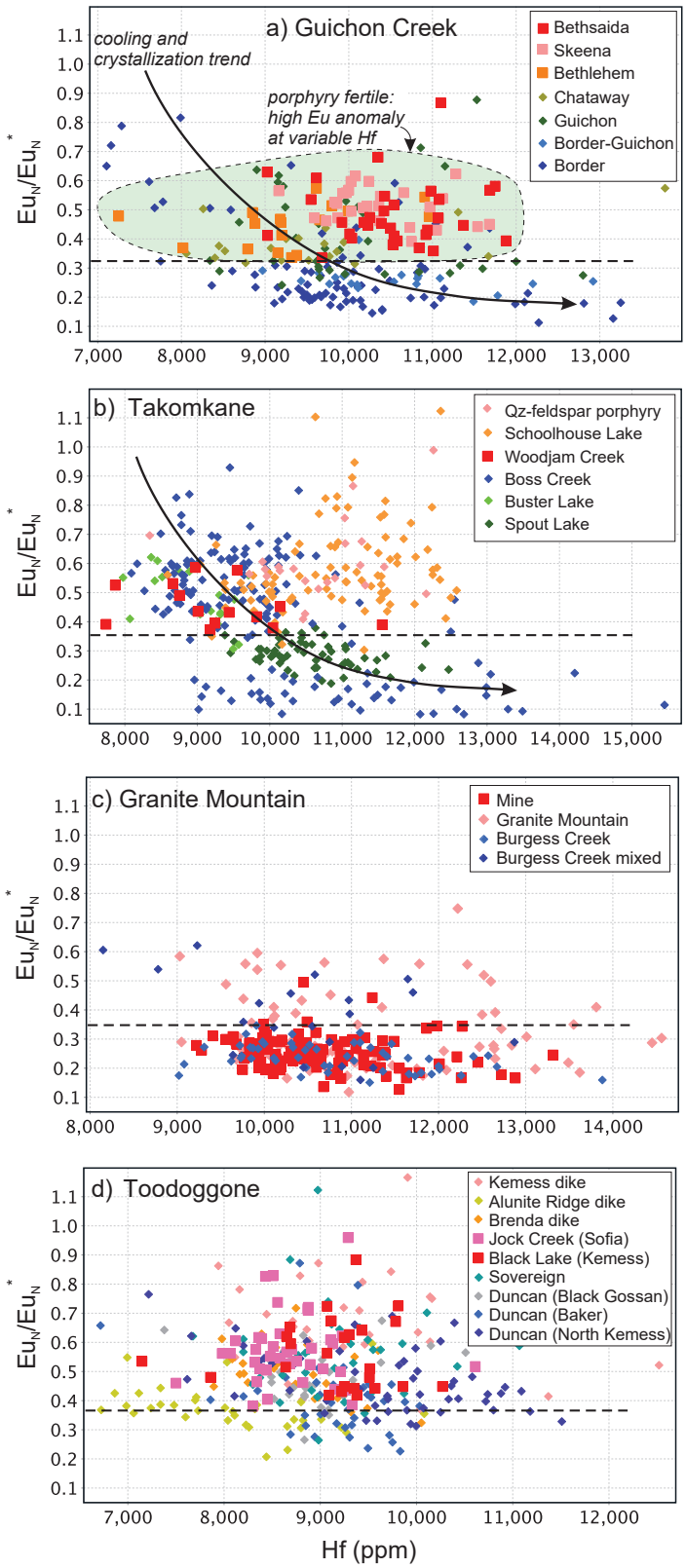

Figure 8: An Eu anomaly (Eu_N/Eu_N^*) versus Hf concentration plot, showing that zircons from mineralized plutons (larger size symbols) have Eu anomaly values that are >0.35 (except Granite Mountain Mine phase) regardless of Hf concentration. Zircons from nonmineralized phases have variable Eu values a) Guichon Creek batholith; b) Takomkane batholith; c) Granite Mountain batholith; d) Toodoggone area.

$Ce_N/Ce_N^* = (Ce_N/(La_N*Pr_N)^{1/2}$ anomaly is difficult (e.g., Dilles et al., 2015). For example, both La and Pr are very low in abundance in zircon and below the detection limit in many of our analyses.

Hafnium is an incompatible element and its content in zircon is used as a proxy for degree of crystallization and generally correlates with a decrease in modal temperature (Dilles et al., 2015). The Eu anomaly versus Hf plot shows distinct variations in BC porphyry-related plutons (Fig. 8a–d).

In the Guichon Creek batholith, zircons from the nonmineralized Border, Guichon and Chataway phases show an increase in Hf concentration as the Eu anomaly decreases; however, most nonmineralized samples have Eu anomalies that are <0.3 (Fig. 8a). Zircons from the mineralized Bethsaida, Skeena and Bethlehem phases have variable Hf concentrations, with samples from the Bethsaida and Skeena phases showing higher Hf concentrations than those from the Bethlehem phase, which suggests that the Bethsaida and Skeena phases formed at lower temperatures than the Bethlehem phase. Lee et al. (2017a; 2020) reported a similar trend. More importantly, zircons from all three mineralized phases have Eu anomalies >0.32, suggesting that magmatic cooling and crystallization in these mineralized phases occurred under higher oxidation states that prevented the decrease in Eu anomaly values, in sharp contrast to values of the nonmineralized phases.

Zircons from the Takomkane batholith show similar Eu and Hf relationships to those of the Guichon Creek zircons. Samples from the Spout Lake, Buster Lake and Boss Creek plutons show zircons with a wide range of Eu anomalies and Hf concentrations that roughly define a curved line (Fig. 8b). Zircons from the mineralized Woodjam Creek unit display a distinct Eu anomaly trend that is >0.35. Zircons from the younger but nonmineralized phases of the Schoolhouse Lake and quartz-feldspar porphyry units also display a cluster of Eu anomaly values >0.35. However, zircons from these two units show a higher Hf concentration relative to that of the Woodjam Creek unit samples, suggesting that magmas were more fractionated in these younger units.

Zircons from the Granite Mountain batholith show the same range of Hf concentrations as those from the Guichon Creek and Takomkane batholiths, but the Eu anomaly values in zircon for the nonmineralized phases and mineralized Mine phase overlap and are mostly low (<0.35), which suggests that much of this batholith crystallized under a low oxidation state (Fig. 8c). Kobylinski et al. (2020) showed similar low values for the Eu anomaly suggesting low oxidation states for this batholith. However, Kobylinski et al. (2020), based on Ce^{4+}/Ce^{3+} and calculated fO_2, showed that mineralized phases of the Granite Mountain batholith were slightly more oxidized (FMQ = +1.7 ± 0.7) relative to barren phases (FMQ = +1.3 ± 0.5). This along with field observations that mineralized porphyry dikes cut the Mine phase (see above), suggests that the so-called Mine phase represents a

multi-phase intrusive body and potentially more oxidized phases have not been exposed.

Zircons from select plutons in the Toodoggone district also show a wide range of Hf concentrations. Zircons from the mineralized phase of the Black Lake plutonic suite at the Kemess mine and from the Jock Creek pluton at the Sofia mineral occurrence show an Eu anomaly that is >0.35. The zircon grains from other phases, such as those from the Duncan and Sovereign plutons, have variable Eu anomaly values that range from 0.2 to >1. Thus, even with significant overlap, the very low Eu anomaly (<0.35) does not occur in zircons of the mineralized phases.

6.4 Oxidation State: Effect of Titanite and Apatite Crystallization or Magmatic Water

The Eu anomaly in zircon is commonly used to characterize the oxidation state of the magma due to the fact that at a higher oxidation state most Eu is present in the trivalent state and is not partitioned into fractionating plagioclase (Frey et al., 1978; Dilles et al., 2015). Alternatively, the lack of a significant Eu anomaly can also be caused by high magmatic water contents, which suppresses plagioclase fractionation (Richards, 2011). Loader et al. (2017) argued that the fractionation of titanite and apatite also has the potential to impart a positive Eu anomaly on residual melts, which may be inherited by zircon when it subsequently crystallizes.

Plots of the Eu anomaly in zircon versus Yb/Gd (Fig. 9) are used here to further characterize the Eu anomaly and the effect of crystal fractionation, oxidation state and magmatic water content. As indicated previously, the Yb/Gd is a proxy for fractionation of apatite, hornblende and titanite, which depletes the melt in MREE causing an increase in zircon of HREE relative to MREE (high Yb/Gd). Zircons from the nonmineralized plutons have a wide range of Eu anomaly values (<0.2 to >0.6) and Yb/Gd (~10 to >40). Zircons from the mineralized plutons, except the Mine phase of the Granite Mountain batholith, display a similar range of Yb/Gd but generally have a distinctly higher Eu anomaly (≥0.35).

The above relationships suggest that apatite and titanite fractionation had different effects on mineralized and nonmineralized plutons. Zircons from the nonmineralized phases of all batholiths show a positive correlation between Yb/Gd and Eu_N/Eu_N^* (Fig. 9a–d). Thus, as the melt became more fractionated with crystallization of apatite and titanite (i.e., higher Yb/Gd), the Eu anomaly increased, becoming less negative. Therefore, the increase in the Eu anomaly could be related to apatite and titanite fractionation, as described by Loader et al. (2017), although the effect of an increase in oxidation state cannot be ruled out. However, the Eu anomaly values of zircons from the mineralized phases do not correlate well with Yb/Gd (Fig. 9). Excepting the Mine Phase, the mineralized phases have an Eu

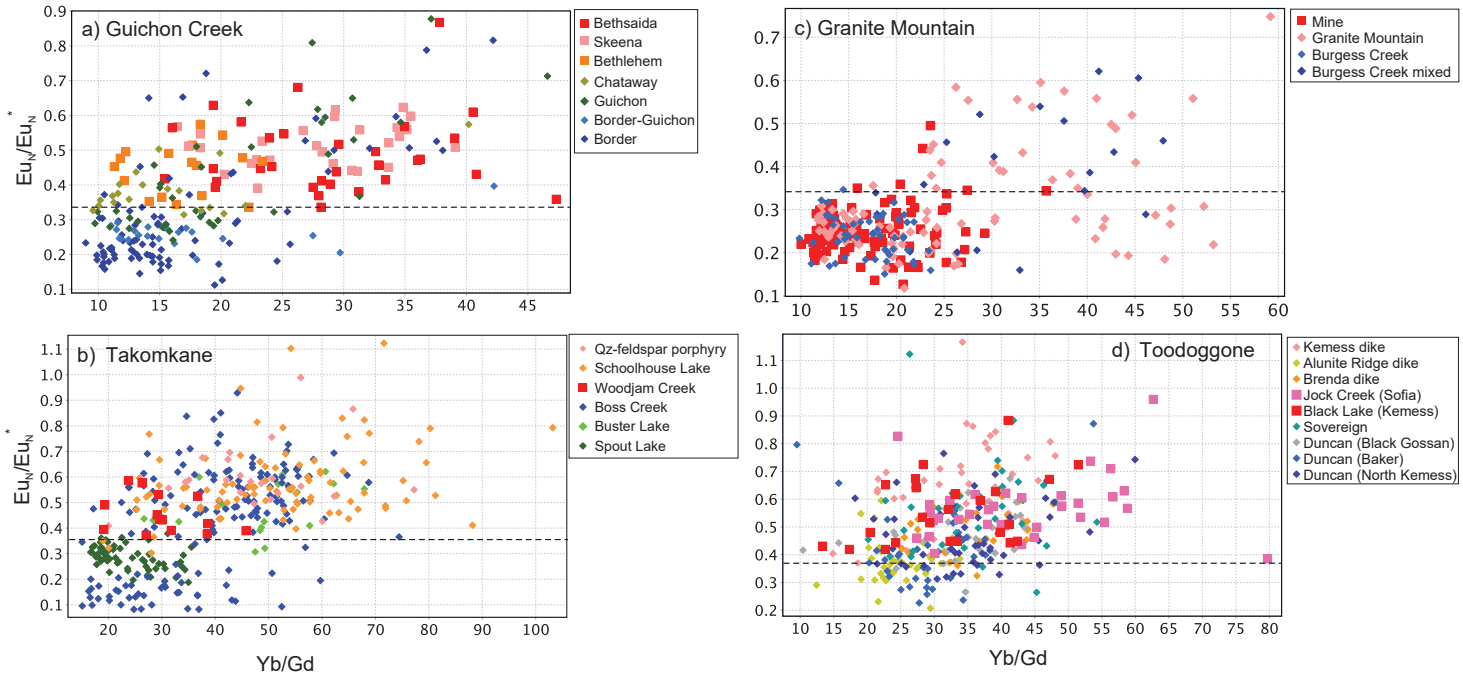

Figure 9: Europium anomaly in zircons versus Yb/Gd, as a proxy for apatite and titanite fractionation, showing that the Eu anomaly values in zircons from the mineralized plutons is not affected by apatite and titanite fractionation: a) Guichon Creek batholith; b) Takomkane batholith; c) Granite Mountain batholith; d) Toodoggone area.

anomaly that is >0.35 whether Yb/Gd are high or low, suggesting that apatite and titanite crystallization did not significantly influence the Eu anomaly in zircons of the mineralized plutons.

The variation in Yb/Gd together with the petrographic evidence indicates that apatite and titanite fractionation occurred in the mineralized plutons but did not affect the Eu anomaly in zircon. It is possible that the effect of apatite and titanite crystallization on the Eu anomaly of zircon was largely minimized or nullified by a high oxidation state and water content of the mineralizing magma. This conclusion is based on the consistently high Eu anomaly at variable Hf concentrations (Fig. 8), that emphasizes the importance of magmatic water content and fluid saturation in porphyry-fertile plutons (see also Dilles et al., 2015).

6.5 Ti-in-Zircon Temperature

The temperature of zircon crystallization can be estimated using the Ti-in-zircon thermometer of Watson and Harrison (2005) and Watson et al. (2006), corrected to an activity of TiO_2=0.7, to reflect titanite and titanomagnetite saturation (Watson and Harrison, 2005; Ferry and Watson, 2007). This Ti-in-zircon temperature allows the trace-element variations of zircon to be viewed as a function of temperature. The Hf content of zircon is an effective proxy for the crystallization of zircon in a melt and typically increases with cooling, whereas REE contents, including Ti, and calculated temperatures, decrease (Watson et al., 2006; Dilles et al., 2015; Lee et al., 2017b).

Despite some scatter in the data, probably due to analytical uncertainties and small variations in the activity of TiO_2, Figure 10 illustrates that increases in the Hf content correlates with decrease in Ti-in-zircon temperature for both fertile and non-mineralized units, in most evaluated plutonic suites. At Guichon Creek, zircons from pre-mineral phases of the batholith have model temperatures ca. 850°C– 700°C (this study; Lee et al., 2020). In contrast, zircon in mineralized phases of the batholith, i.e., Bethlehem, Skeena and Bethsaida, yield lower model temperatures ca. 750°C–600°C consistent with zircon crystallization in near-eutectic conditions close to the solidus of hydrous granite (this study, Fig. 10a; Lee et al., 2020). Within the mineralized phases, the Bethlehem phase was ca. 100–150°C hotter than Skeena and Bethsaida phases.

Zircons from the Takomkane batholith show similar trends of Hf and Ti-in-zircon temperature. Zircons from the Spout Lake pluton yielded temperatures >750°C whereas zircons from other phases of the batholith, including both mineralized and nonmineralized, yield model temperatures <750°C (Fig. 10b).

Zircons from all phases of Granite Mountain batholith yield temperatures ca. 850°C–600°C with no distinction between mineralized and nonmineralized phases of the batholith (this study; Kobylinski et al., 2020). Moreover, most of zircon's calculated temperatures were above the eutectic temperature (ca. 750°C). This is different compared to all of the other mineralized batholiths, except the Spout Lake pluton which has elevated tempera-

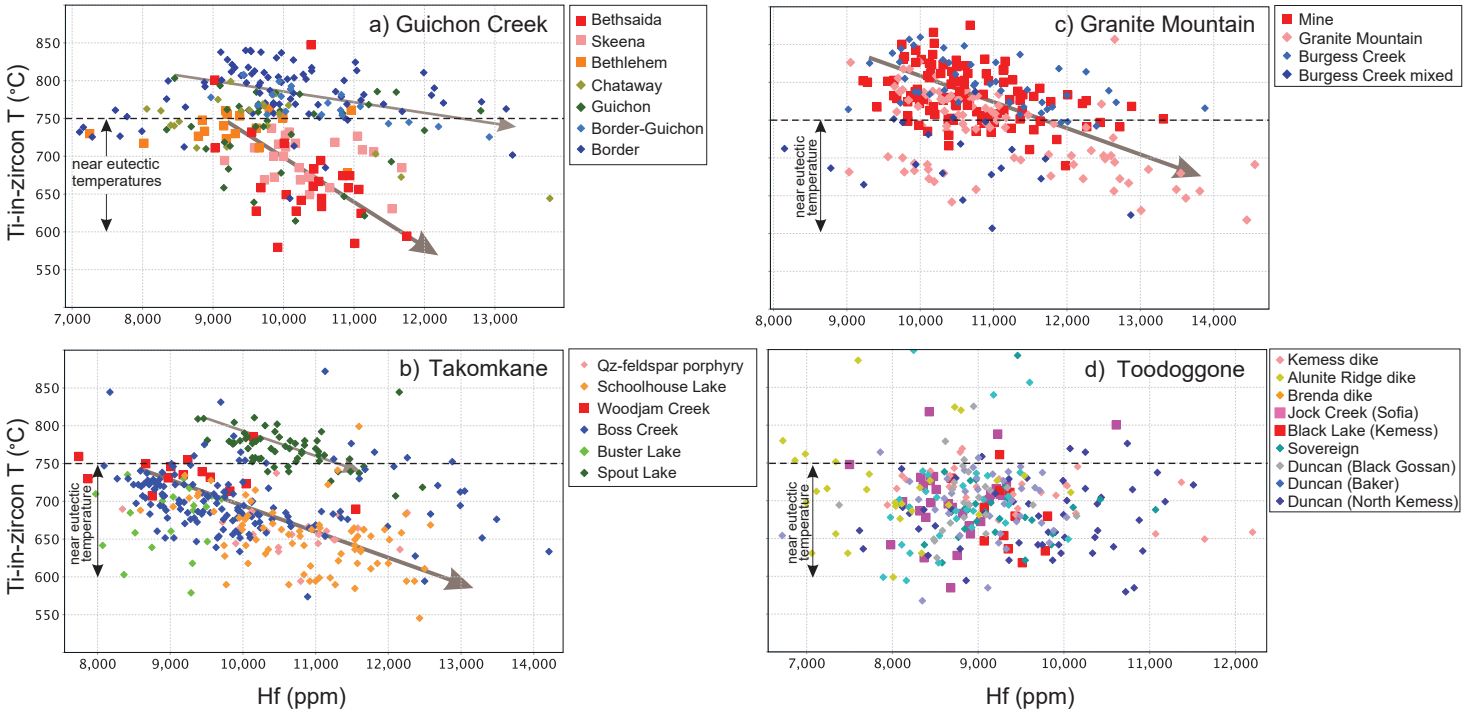

Figure 10: Ti-in-zircon temperatures versus Hf plot. Temperatures calculated assuming a melt activity of TiO2 = 0.7, after Ferry and Watson (2007). Most mineralizing plutons (except the Granite Mountain) yield temperatures of 750°C to 600°C, coincident with conditions close to the solidus of hydrous granite. Nonmineralized plutons yield similar or higher temperatures.

tures of ca. 750°C, and further suggests that the studied samples of the Granite Mountain Mine phase is probably not the main causative porphyry phase (see also Kobylinski et al., 2020). Field observations and evidence from Eu anomalies further support this possibility.

Toodoggone district zircons do not show distinct temperature variation with regard to Hf concentration. This could be due to the limited number of samples analyzed from each phase, however, most of the analyzed zircon grains yielded model temperatures <750 °C (ca. 600–750°C).

Results from the calculated Ti-in-zircon temperatures suggest that mineralized porphyry plutons yield model temperatures that are <750°C, which is consistent with zircon crystallization from magmas with near-eutectic conditions close to the solidus of hydrous granite (e.g., Dilles et al., 2015). However, this is not unique to just the mineralized porphyry bodies because some nonmineralized porphyry units may have also crystallized below 750°C. Therefore, although eutectic temperatures of crystallization of magmas is an important factor in the generation of the porphyry-type mineralization, other factors such as oxidation state, water, sulphur and copper budget of the melt are equally critical.

6.6 Correlation Between Trace-Element and Zircon Texture

Zircon grains can display complex and fine textural zoning. The correlation between these textures and zircon chemistry is usually difficult to establish because of the fine nature of the textural variations in zircon (<10 µm) and the laser-beam size selected for LA-ICP-MS analysis (34 µm in this case). However, this study shows that there is a correlation between the type of zircon grains and their trace-element chemistry. Figure 11a shows the Eu anomaly plotted against Hf content for all studied zircon grains, classified according to their type of zoning. Zircon grains with an elongated shape and tabular zoning have distinctly lower Eu anomaly values, whereas zircon grains with oscillatory zoning display a wide range and higher Eu anomaly values (≥0.35). Zircon grains that display tabular-oscillatory zoning typically have similar compositions to those with tabular zoning; however, some zircon grains have elevated Eu anomaly values like oscillatory zoned zircons. The reason for this relationship is an artifact since the cores were mostly analysed in the tabular-oscillatory grains since the rims were typically too narrow and only analyzed if thick enough (>40 microns).

U-Pb age calculations for a subset of grains (Fig. 11b) show that zircon grains with tabular zoning and a low Eu anomaly are notably older than 195 Ma. The zircon grains with oscillatory zoning and a high Eu anomaly have a wide range of ages but their abundance shows a reverse relationship with age. This relationship suggests that the plutons emplaced between 200–185 Ma (i.e., Early Jurassic porphyry belts) are more dominantly characterized by high Eu anomalies whereas those older (i.e., Late Triassic) contain plutons with mix of zircons showing low Eu anomalies (tabular) and high Eu anomalies (oscillatory zoning).

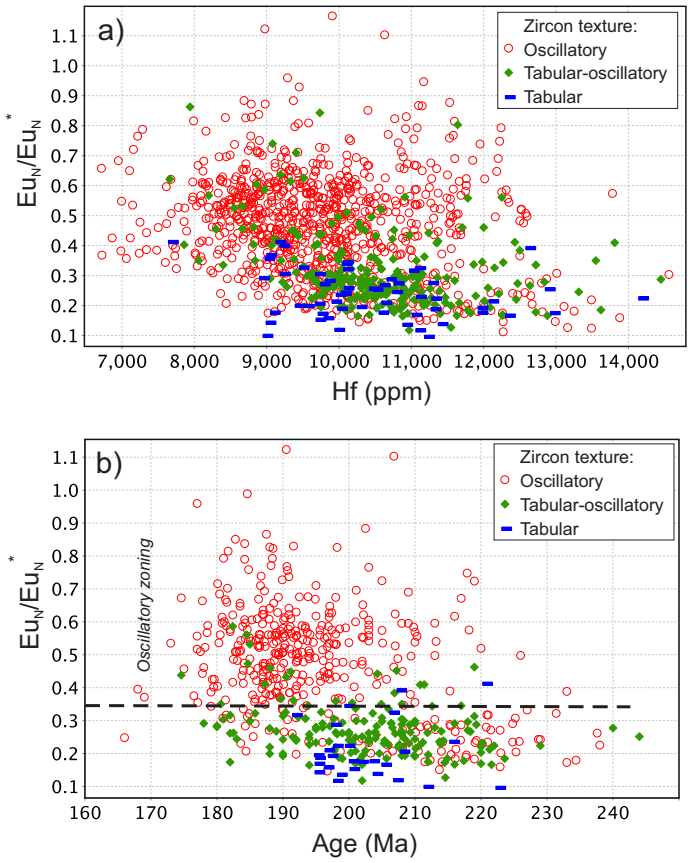

Figure 11: Diagram showing the distribution of zircon textures; a) Europium anomaly in zircon versus Hf plot; b) Europium anomaly in zircon versus age plot. Zircons with higher Eu anomaly commonly show oscillatory zoning whereas zircons with tabular or tabular-oscillatory zoning have a lower Eu anomaly and are older.

Zircon grains with oscillatory zoning either show regular zoning (Fig. 6a) or irregular zoning (Fig. 6e,f) characterized by new growth zones that truncate or even crosscut older oscillatory zones. Figure 12a,b shows the compositional differences of zircons with regular and irregular zoning from the Guichon Creek batholith. Zircons with irregular oscillatory zoning occur within the Border phase, Guichon and Chataway phases. These zircons show a trend of a decreasing Eu anomalies with increasing Hf concentrations, i.e., crystallization of magma (Fig. 12a). Zircons with regular oscillatory zoning occur in all rock types of the Guichon Creek batholith. Such zircons have high (>9000 ppm) Hf concentrations and their Eu anomaly values lack distinct variations with Hf concentrations (Fig. 12b). More importantly, nearly all the zircons from the Bethlehem, Skeena and Bethsaida phases, (i.e., the mineralized phases of the Guichon Creek batholith) show regular oscillatory zoning and the zircons have Eu anomaly values of >0.35 (Fig. 12b). Zircons from the

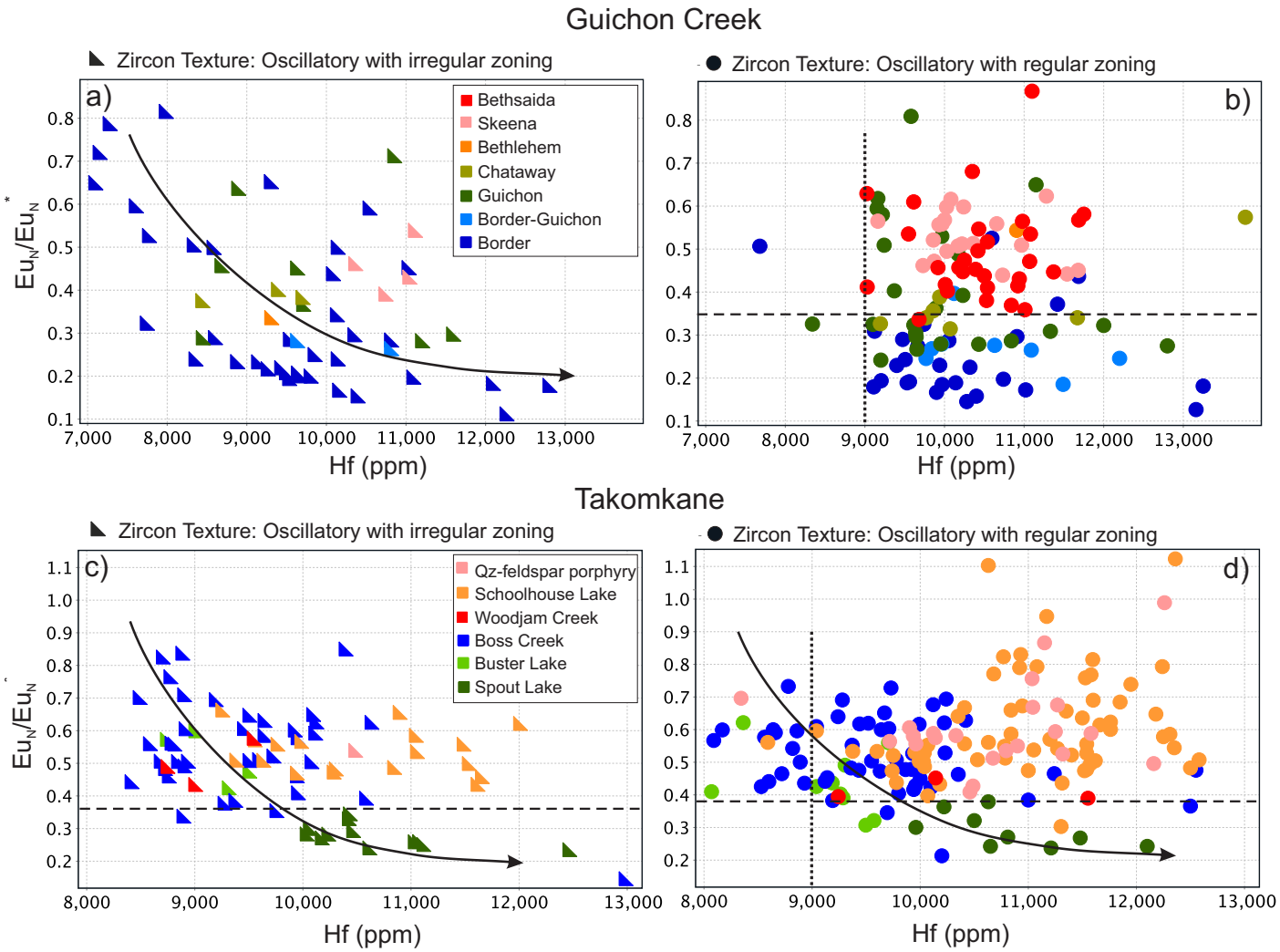

Figure 12: Distribution of regular oscillatory zoned zircon and irregular zoned zircon; a) Guichon Creek zircons with irregular oscillatory zoning show variable Eu anomaly values correlating with Hf concentration; b) Guichon Creek zircons with regular oscillatory zoning are characterized by high (>9000 ppm) Hf concentrations and no linear relationship except elevated Eu anomaly values corresponding to mineralized phases; c) and d) Zircons from Takomkane batholith show overlapping relationships of zircons with higher Eu anomaly and higher Hf concentrations are commonly those with regular oscillatory zoning.

other batholiths studied show mixed relationships with regard to the regular versus irregular oscillatory zoning. For example, zircon grains with both regular and irregular zoning from Takomkane batholith show a decreasing trend of the Eu anomaly with increasing Hf concentrations, whereas others do not (Fig. 12c,d). However, within this mixture it is apparent that zircons with higher Eu anomaly values and higher Hf concentrations typically have regular oscillatory zoning (Fig. 12d).

It is beyond the scope of this report to discuss the causes of regular or irregular zoning in zircon (e.g., Gagnevin et al., 2010; Geisler et al., 2007). However, comparison of Figures 10 and 12 suggests that zircons with regular oscillatory zoning are more abundant at near-eutectic temperatures (<750°C). This is particularly critical in terms of the magma oxidation state and magmatic water content suggesting that zircons with regular oscillatory zoning are formed at favourable magmatic temperature, oxidation state and water content of magma for the generation of porphyry mineralization compared to zircons with other textures. Therefore, the shape and texture of zircon grains can be used as indicators to screen plutons for fertility.

7. CONCLUSIONS

Zircons from porphyry-fertile batholiths in BC have characteristics that record distinct chemical and physical properties that indicate an increased potential to generate porphyry copper deposits. Zircons from mineralized phases of the Guichon Creek and Takomkane batholiths and Toodoggone area have small negative Eu anomalies (Eu_N/Eu_N^* ≥0.35). These values reflect: 1) high magmatic water content and consequent suppression of early plagioclase crystallization (e.g., Ballard et al., 2002); and 2) late magmatic oxidation that results in the loss of SO_2-rich magmatic-hydrothermal ore fluids during late-stage crystallization of

granite (Dilles et al., 2015; Lee et al., 2017b). Zircons from the mineralized Mine Phase of the Granite Mountain have negative Eu anomalies (Eu_N/Eu_N* 0.2–0.35).

The similar low Th/U and high Yb/Gd ratios of zircons from mineralized phases suggest that the fertile magmas were formed from a fractionated melt. Similarly, Ti-in-zircon model temperatures, with the exception of the Mine phase, Granite Mountain, indicate that fertile plutons yield lower model temperatures ca. 750°C–600°C consistent with zircon crystallization in near-eutectic conditions at close to the solidus of hydrous granite melt. Zircon crystallization temperatures determined from the mineralized Mine phase yield temperatures ca. 850°C–750°C. Results of this study show the importance of factors other than crystal fractionation and cooling for generating fertile magmas.

In each magmatic complex that forms a batholith, the mineralized magmatic phases or plutons are associated with pre- and post-mineral plutons that are poorly mineralized or nonmineralized. These nonmineralized plutons show variable Eu anomaly values, which are interpreted to reflect crystal fractionation, particularly apatite and titanite (Loader et al., 2017). Therefore, crystal fractionation within these magmas alone does not produce ore deposits, particularly if the magma has a low oxidation state or low magmatic water content, or both. Crystal fractionation also accompanied cooling of the mineralized plutons, but unlike the nonmineralized plutons, the effects of apatite and titanite crystallization were suppressed by a high oxidation state which itself probably resulted from high water content of the magma and SO2 degassing (Dilles et al., 2015). Therefore, an Eu anomaly distribution in plutons that is not significantly affected by Hf concentration or Yb/Gd values (i.e., crystal fractionation), suggests that oxidation state and magmatic water content were significantly high during the cooling history of the magma. This distinct chemical character of zircons identifies plutons that are capable of forming porphyry copper deposits.

Also important is the correlation of zircon textures with composition and fertility. Zircons from fertile plutons have oscillatory zoning with notable but thin irregular textures at their rims whereas nonmineralized plutons have tabular or oscillatory zoning commonly with irregular textures. The correlation of regular oscillatory zoned zircons with high Eu anomaly values (>0.35) and high Hf concentration (>9000 ppm) suggests that oxidized, cooled (<750°C), wet magmas promote regular oscillatory zoning. Such zircons locally show narrow irregular rims that truncate and crosscut earlier growth zones (see Fig. 6a) which are interpreted to be related to local dissolution–recrystallization process. On the other hand, less oxidized, hotter and drier melts promote zircons with tabular and irregular oscillatory zoning. Despite some overlap in the data sets, recognition of these important zircon textures can provide a quick method to estimate and evaluate the fertility characteristics of the host rocks.

In summary, the key features of zircon that indicate porphyry-fertile plutons in BC are:

- zircons with oscillatory zoning, particularly those with regular zoning patterns;
- zircons with evidence of simple crystal fractionation, with values on the Yb/Gd versus Th/U curve which suggest fractionation without crustal contamination;
- zircons with Ti-in-zircon model temperatures <750°;
- zircons with Eu anomaly values ≥0.35 that suggest a high oxidation state and high magmatic water content; and
- zircons with Eu anomaly values that are not dependent on Hf concentration or Yb/Gd values, suggesting that magmatic water content and oxidation state were high and remained high during much of the magma crystallization.

8. ACKNOWLEDGMENTS

Geoscience BC is thanked for its financial contribution in support of this project. B. Najafian helped with mineral separation, E. Chan helped with mineral-grain photography and H. McIntyre helped with LA-ICP-MS analysis. Edith Czech and Marghaleray Amini from the Pacific Centre for Isotopic and Geochemical Research (PCIGR), UBC, helped with the EPMA and LA-ICP-MS analyses, respectively. Johanna McWhirter assisted with project management and final editing. Two anonymous reviwers provided useful comments on an earlier version of this report. Shannon Guffey and Sara Jenkins assisted with final figures and layout.

9. REFERENCES

Ash, C.H., Rydman, M.O., Payne, C.W. and Panteleyev, A., 1999, Geological setting of the Gibraltar mine, south-central British Columbia (93B/8, 9); in Exploration and Mining in British Columbia 1998, BC Ministry of Energy and Mines, BC Geological Survey, p. A1–A15.

Audétat, A., and Simon, A.C., 2012, Magmatic controls on porphyry Cu genesis: Society of Economic Geologists, Special Publication 16, p. 553–572.

Averill, S.A., 2011, Viable indicator minerals in surficial sediments for two major base metal deposit types: Ni-Cu-PGE and porphyry Cu; Geochemistry, Exploration, Environment, Analysis, v. 11, p. 279–291.

Ballard, J.R., Palin, J.M. and Campbell, I.H., 2002, Relative oxidation states of magmas inferred from Ce(IV)/Ce(III) in zircon: application to porphyry copper deposits of northern Chile; Contributions to Mineralogy and Petrology, v. 144, p. 347–364.

Banik, T. J., Coble, M.A. and Miller, C.F., 2017, Porphyry Cu formation in the middle Jurassic Yerington batholith, Nevada, USA: Constraints from laser Raman, trace element, U-Pb age, and oxygen isotope analyses of zircon; Geosphere, v. 13, no. 4, p. 1113–1132

Belousova, E.A., Griffin, W.L., and O'Reilly, S.Y., 2006, Zircon crystal morphology, trace element signatures and Hf isotope composition as a tool for petrogenetic modeling: examples from Eastern Australian granitoids. Journal of Petrology, v. 47, v. 329–353

Belousova, E.A., Griffin, W.L., O'Reilly, S.Y., and Fisher, N.I., 2002, Igneous zircon: trace element composition as an indicator of source rock type; Contributions to Mineralogy and Petrology, v. 143, p. 602–622

Bissig, T. and Cooke, D.R., 2014, Introduction to the special issue devoted to alkalic porphyry Cu-Au and epithermal Au deposits; Economic Geology v. 109, p. 819–825.

Bouzari, F., Bissig, T., Hart, C.J.R., Leal-Mejía, H., 2019, An Exploration Framework for Porphyry to Epithermal Transitions in the Toodoggone Mineral District (94E); Geoscience BC Report 2019-08, MDRU Publication 424, 101 p. URL http://www.geosciencebc.com/wp-content/uploads/2019/11/Geoscience-BC-Report-2019-08.pdf [December 2019]

Bouzari, F., Hart, C.J.R., Bissig, T., and Lesage, G., 2018, Mineralogical and Geochemical Characteristics of Porphyry-Fertile Plutons: Guichon Creek, Takomkane and Granite Mountain Batholiths, south-central British Columbia (NTS 092I, P, 093A, B); Geoscience BC Report 2018-17, MDRU Publication 412, 36 p. URL < http://cdn.geosciencebc.com/project_data/GBCR2018-17/GBCreport2018-17.pdf> [November 2019]

Burnham, C.W., and Ohmoto, H., 1980, Late-stage processes of felsic magmatism, in Granitic Magmatism and Related Mineralization, Ishihara, S., and S. Takenouchi (eds.); Mining Geology Special Issue 8, p. 1–11

Byrne, K., Stock, E., Ryan, J., Johnson, C., Nisenson, J., Alva Jimenez, T., Lapointe, M., Stewart, H., Grubisa, G. and Sykora, S., 2013, Porphyry Cu-(Mo) deposits in the Highland Valley district, south-central British Columbia; in Porphyry Systems of Central and Southern BC, Tour of Central BC Porphyry Deposits from Prince George to Princeton, J. Logan. and T. Schroeter (eds.); Society of Economic Geologists, Field Guidebook Series, v. 44, p. 99–116.

Bysouth, G.D., Campbell, K.V., Barker, G.E. and Gagnier, G.K., 1995, Tonalite trondhjemite fractionation of peraluminous magma and the formation of syntectonic porphyry copper mineralization, Gibraltar mine, central British Columbia; in Porphyry Deposits of the Northwestern Cordillera of North America, T.G. Schroeter (ed.); Canadian Institute of Mining, Metallurgy and Petroleum, Special Volume 46, p. 201–213.

Casselman, M.J., McMillan, W.J. and Newman, K.M., 1995, Highland Valley porphyry copper deposits near Kamloops, British Columbia: a review and update with emphasis on the Valley deposit; in Porphyry Deposits of the Northwestern Cordillera of North America, T.G. Schroeter (ed.); Canadian Institute of Mining and Metallurgy, Special Volume 46, p. 161–191.

Cherniak, D.J., and Watson, E.B., 2003, Diffusion in zircon; Reviews in Mineralogy and Geochemistry, v. 53, p. 113–143

Cherniak, D.J., Hanchar, J.M., and Watson, E.B., 1997, Diffusion of tetravalent cations in zircon; Contributions to Mineralogy and Petrology, v. 127, p. 383–390

Chiaradia, M., Schaltegger, U., Spikings, R., Wotzlaw, J.-F. and Ovtcharova, M., 2013, How accurately can we date the duration of magmatic-hydrothermal events in porphyry systems?–An invited paper; Economic Geology, v. 108, p. 565–584.

D'Angelo, M., Miguel, A., Hollings, P., Byrne, K., Piercey, S. and Creaser, R., 2017, Petrogenesis and Magmatic Evolution of the Guichon Creek Batholith: Highland Valley Porphyry Cu±(Mo) District, South-Central British Columbia; Economic Geology, v. 112, p. 1857–1888.

del Real, I., Bouzari, F, Rainbow, A., Bissig, T., Blackwell, J, Sherlock, R., Thompson, J.F.H. and Hart, C.J.R., 2017, Spatially and temporally associated porphyry deposits with distinct Cu/Au/Mo ratios, Woodjam district, central British Columbia; Economic Geology, v. 112, p. 1673–1717.

Diakow, L. J., 2006, Geology between the Finlay River and Chukachida Lake, Central Toodoggone River Map Area, North-central British Columbia (Parts of NTS 94E/2, 6, 7, 10 and 11); B.C. Ministry of Energy, Mines and Petroleum Resources, Open File Map 2006-4, 1:50 000 scale

Diakow, L.J., 1990, Volcanism and evolution of the Early and Middle Jurassic Toodoggone Formation, Toodoggone mining district, British Columbia. Unpublished Ph.D. thesis, The University of Western Ontario, 178 p.

Diakow, L.J., Nixon, G.T., Rhodes, R. and Lane, B., 2005, Geology between the Finlay and Toodoggone rivers, Toodoggone river map area, north-central British Columbia (parts of NTS 94E/2, 6 and 7); British Columbia Ministry of Energy, Mines and Petroleum Resources, Open file map 2005-3, 1:50 000 scale, URL <http://www.empr.gov.bc.ca/mining/geoscience/publicationscatalogue/openfiles/2005/pages/2005-3.aspx> [November 2019].

Diakow, L.J., Panteleyev, A. and Schroeter, T.G., 1993, Geology of the Early Jurassic Toodoggone Formation and gold-silver deposits in the Toodoggone River map area, northern British Columbia; British Columbia Ministry of Energy, Mines and Petroleum Resources, 72 p., URL <http://www.empr.gov.bc.ca/Mining/Geoscience/PublicationsCatalogue/Bul-

letinInformation/BulletinsAfter1940/Documents/Bull86.pdf> [November 2019].

Diakow, L.J., Panteleyev, A., Schroeter, T.G., 1991, Jurassic epithermal prospects in the Toodoggone river area, northern British Columbia: examples of well preserved, volcanic-hosted, precious metal mineralization; Economic Geology, v. 86, p. 529–554

Dilles, J.H., and Einaudi, M.T., 1992, Wall-rock alteration and hydrothermal flow paths about the Ann-Mason porphyry copper deposit, Nevada: a 6-km vertical reconstruction; Economic Geology, v. 87, p. 1963–2001.

Dilles, J.H., Kent, A.J.R., Wooden, J.L., Tosdal, R.M., Koleszar, A., Lee, R.G. and Farmer, L.P., 2015, Zircon compositional evidence for sulfur-degassing from ore-forming arc magmas; Economic Geology, v. 110, p. 241–251.

Duuring, P., Rowins, S.M., McKinley, B.S.M., Dickinson J.M., Diakow, L.J., Kim, Y-S. and Creaser, R.A., 2009, Magmatic and structural controls on porphyry-style Cu–Au–Mo mineralization at Kemess South, Toodoggone district of British Columbia, Canada; Mineralium Deposita, v. 44, p. 463–496.

Ferry, J.M., and Watson, E.B., 2007, New thermodynamic models and revised calibrations for the Ti-in-zircon and Zr-in-rutile thermometers; Contributions to Mineralogy and Petrology, v. 154, p. 429–437

Frey, F.A., Chappell, B.W. and Roy, S.D., 1978, Fractionation of rare-earth elements in the Tuolumne Intrusive Series, Sierra Nevada batholith, California; Geology, v. 6, p. 239–242.

Gagnevin, D., Daly, J.S. and Kronz, A., 2010, Zircon texture and chemical composition as a guide to magmatic processes and mixing in a granitic environment and coeval volcanic system; Contributions to Mineralogy and Petrology, v.159, p. 579–596

Geisler, T., Schaltegger, U., Tomaschek, F., 2007, Re-equilibration of zircon in aqueous fluids and melts; Elements, v. 3, p. 43–50

Hanchar, J.M., and Miller, C.F., 1993, Zircon zonation patterns as revealed by cathodoluminescence and backscattered electron images: Implications for interpretation of complex crustal histories; Chemical Geology, v. 110, p. 1–13

Harding, B., 2012, The characterization of molybdenum mineralization at the Gibraltar mines Cu-Mo porphyry, central British Columbia. Unpublished B.Sc. thesis, Queen's University, Kingston, Ontario, 52 p.

Harrison, T.M., and Watson, E.B., 1983, Kinetics of zircon dissolution and zirconium diffusion in granitic melts of variable water content; Contributions to Mineralogy and Petrology, v. 84, p. 67–72

Hoskin, P.W.O., 2005, Trace-element composition of hydrothermal zircon and the alteration of Hadean zircon from the Jack Hills, Australia; Geochimica et Cosmochimica Acta, v. 69: p. 637–648

Jackson, S.E., Gunther, D. and Sylvester, P.J., 2003, Applications of laser-ablation ICP-MS analysis: A tribute to Henry P. Longerich; Canadian Mineralogist, v. 41, p. 257–258.

Kobylinski, C., Hattori, K., Smith, S., and Plouffe, A., 2020, Protracted magmatism and mineralized hydrothermal activity at the Gibraltar porphyry copper-molybdenum deposit, British Columbia. Economic Geology, doi: 10.5382/econgeo.4724. [July 2020].

Lee, R.G., Byrne, K., Alfaro, M., D'Angelo, M., Hart, C.J.R., Hollings, P. and Gleeson, S.A., Alfaro, M., 2020, Using zircon trace element composition to assess porphyry copper potential of the Guichon Creek batholith and Highland Valley Copper deposit, south-central B.C.; Mineralium Deposita, doi: 10.1007/s00126-020-00961-1 [December 2019].

Lee, R.G., Byrne, K., Alfaro, M., D'Angelo, M., Hart, C.J.R., Hollings, P. and Gleeson, S.A., 2017a, Assessing the zircon compositional evolution from the Guichon Creek Batholith and Highland Valley Copper deposit, south-central B.C.: Abstract, Mineral Resources to Discover - 14th SGA Biennial Meeting 2017.

Lee, R.G., Dilles, J.H., Tosdal, R., Wooden, J.L. and Mazdab, F.K., 2017b, Magmatic evolution of granodiorite intrusions at the El Salvador porphyry copper deposit, Chile, based on trace element composition and U/Pb age of zircons; Economic Geology, v. 112, p. 245–273.

Loader, M.A., Wilkinson, J.J. and Armstrong R.N., 2017, The effect of titanite crystallisation on Eu and Ce anomalies in zircon and its implications for the assessment of porphyry Cu deposit fertility; Earth and Planetary Science Letters, v. 472. p. 107–119.

Logan, J.M. and Mihalynuk, M.G., 2014, Tectonic controls on early Mesozoic paired alkaline porphyry deposit belts (Cu-Au±Ag-Pt-Pd-Mo) within the Canadian Cordillera; Economic Geology, v. 109, p. 827–858.

Lowery Claiborne. L., Miller, C.F., Walker, B.A., Wooden, J.L., Mazdab, F.K., Bea, F., 2006, Tracking magmatic processes through Zr/Hf ratios in rocks and Hf and Ti zoning in zircons: an example from the Spirit Mountain batholith, Nevada; Mineral Magazine, v. 70, p. 517–543

McMillan, W.J., Anderson, R.G., Chan, R. and Chow, W., 2009, Geology and mineral occurrences (MINFILE), the Guichon Creek Batholith and Highland Valley porphyry copper district, British Columbia; Geological Survey of Canada, Open File 6079, 2 maps, URL <http://geogratis.gc.ca/api/en/nrcan-rncan/ess-sst/78e93fdd-50d0-5877-a024-310362144149.html> [November 2019].

Miller, J.S. and Wooden, J.L., 2004, Residence, resorption and recycling of zircons in Devils Kitchen Rhyolite, Coso volcanic

field, California; Journal of Petrology, v. 45, p. 2155–2170.

Mortensen, J.K., Ghosh, D.K., Ferri, F., 1995, U–Pb geochronology of intrusive rocks associated with copper–gold porphyry deposits in the Canadian Cordillera, in Porphyry Deposits of the Northwestern Cordillera of North America, T.G. Schroeter (ed.); Canadian Institute of Mining and Metallurgy, Special Volume 46, p. 40–57.

Mostaghimi, N., 2016, Structural geology and timing of deformation at the Gibraltar copper-molybdenum porphyry deposit, south-central British Columbia; Unpublished M.Sc. Thesis, The University of British Columbia, 358 p.

Panteleyev, A., 1978, Granite Mountain project (93B/8); in Geological Fieldwork 1977, BC Ministry of Energy, Mines and Petroleum Resources, BC Geological Survey, Paper 1977-1, p. 39–42.

Pouchou, J.L., and Pichoir, F., 1985, PAP f(rZ) procedure for improved quantitative microanalysis, in Microbeam analysis, J.T. Armstrong (ed.), San Francisco, CA, San Francisco Press, p.104–106.

PwC Canada, PricewaterhouseCoopers, 2019, www.pwc.com [November 2019].

Richards, J.P., 2011, High Sr/Y magmas and porphyry Cu±Mo±Au deposits: Just add water; Economic Geology, v. 106, p. 1075–1081.

Sánchez, M.G., Bissig, T. and Kowalcyzk, P., 2015, Toward an improved basis for beneath-cover mineral exploration in the QUEST area, central British Columbia: new structural interpretation of geophysical and geological datasets (NTS 093A, B, G, H, J, K, N); Geoscience BC Report 2015-15. URL < http://cdn.geosciencebc.com/project_data/GBCReport2015-15/ExecutiveSummary_2015_015.pdf> [November 2019]

Schiarizza, P., 2015, Geological setting of the Granite Mountain batholith, south-central British Columbia; in Geological Fieldwork 2014, BC Ministry of Energy, Mines and Petroleum Resources, BC Geological Survey, Paper 2015-1, p. 19–39, URL <http://www.empr.gov.bc.ca/Mining/Geoscience/PublicationsCatalogue/Fieldwork/Documents/2014/02_Schiarizza.pdf> [November 2019].

Schiarizza, P., Bell, K. and Bayliss, S., 2009, Geology and mineral occurrences of the Murphy Lake area, south-central British Columbia (NTS 093A/03); in Geological Fieldwork 2008, BC Ministry of Energy, Mines and Petroleum Resources, BC Geological Survey, Paper 2009-1, p. 169–188, URL <http://www.empr.gov.bc.ca/Mining/Geoscience/PublicationsCatalogue/Fieldwork/Documents/2008/15_Schiarizza.pdf> [November 2019].

Schiarizza, P., Israel, S., Heffernan, S., Boulton, A., Bligh, J., Bell, K., Bayliss, S., Macauley, J., Bluemel, B., Zuber, J., Friedman, R.M., Orchard, M.J., and Poulton, T.P., 2013, Bedrock Geology between Thuya and Woodjam creeks, south-central British Columbia, NTS 92P/7, 8, 9, 10, 14, 15, 16; 93A/2, 3, 6; British Columbia Geology Open File 2013-05. URL < http://cmscontent.nrs.gov.bc.ca/geoscience/PublicationCatalogue/OpenFile/BCGS_OF2013-05.pdf> [November 2019]

Shen, P., Hattori, K., Pan, H., Jackson, S. and Seitmuratova, E., 2015, Oxidation condition and metal fertility of granitic magmas: zircon trace-element data from porphyry Cu deposits in the Central Asian orogenic belt; Economic Geology, v. 110, p. 1861–1878.

Shu, Q., Chang, Z., Lai, Y., Hu, X., Wu, H., Zhang, Y., Wang, P., Zhai, D., and Zhang, C., 2019, Zircon trace elements and magma fertility: insights from porphyry (-skarn) Mo deposits in NE China; Mineralium Deposita, v. 54, p. 645–656.

Spencer, C.J., Kirkland, C.L., Taylor, R.J.M., 2016, Strategies towards statistically robust interpretations of in situ U-Pb zircon geochronology; Geoscience Frontiers v. 7, p. 581-589

Thomas, J., Bodnar, R.J., Shimizu, N., and Sinha, A., 2002, Determination of zircon/melt trace element partition coefficients from SIMS analysis of melt inclusions in zircon; Geochimica et Cosmochimica Acta, v. 66, p. 2887-2901.

Wang, X., Griffin, W.L., O'Reilly, S.Y., Zhou, X.M., Xu, X.S., Jackson, S.E., and Pearson, N.J., 2002, Morphology and geochemistry of zircons from late Mesozoic igneous complexes in coastal SE China: implications for petrogenesis; Mineralogical Magazine, v. 66, p. 235–251

Wark, D.A., and Miller, C.F., 1993, Accessory mineral behavior during differentiation of a granite suite: monazite, xenotime and zircon in the Sweetwater Wash pluton, southeastern California, USA; Chemical Geology, v. 110, p. 49–67

Watson, E.B., and Harrison, T.M., 2005, Zircon thermometer reveals minimum melting conditions on earliest Earth; Science, v. 308, p. 841–844.

Watson, E.B., Wark, D.A., and Thomas, J.B., 2006, Crystallization thermometers for zircon and rutile; Contributions to Mineralogy and Petrology, v. 151, p. 413–433.

Woodsworth, G.J., Anderson, R.G., Brookfield, A. and Tercier, P., 1988, Distribution of Plutonic Suites in the Canadian Cordillera; Geological Survey of Canada, Open File 1982